SPATIAL AND TEMPORAL VARIABILITY OF VERTICAL HYDROLOGIC FLUXES AT THE SAN PEDRO RIVER, AZ

By

Carlos Daniel Soto López

A Thesis Submitted to the Faculty of the

DEPARTMENT OF HYDROLOGY AND WATER RESOURCES

In Partial Fulfillment of the Requirements
For the Degree of

MASTER OF SCIENCE
WITH A MAJOR IN HYDROLOGY

In the Graduate College

THE UNIVERSITY OF ARIZONA

2008

STATEMENT BY AUTHOR

This thesis has been submitted in partial fulfillment of requirements for an advance degree at The University of Arizona and is deposited in the University Library to be made available to borrowers under rules of the Library.

Brief quotations from this thesis are allowed without special permission, provided the accurate acknowledgement of source is made. Request for permission for extend quotation from or reproduction of this manuscript in whole or in part may be granted by the head of the major department or the Dean of the Graduate College when in his or her judgment the proposed use of the material is in the interest of scholarship. In all other instances, however, permission must be obtained from the author.

SIGNED: Carlos Daniel Soto López

APPROVAL BY THE THESIS DIRECTOR

This thesis has been approved on the date shown below:

Dr. Thomas Meixner Professor of Hydrology	06/06/2008 Date

ACKNOWLEDGEMENTS

I would like to thank my advisor and members of the committee for you help and support. I would also like to thank the Bureau of Land Management (BLM), the Agricultural Research Service (ARS) and San Pedro Riparian National Conservation Area (SPRNCA) for access and cooperation. As well as, all my fellow students who helped with the sampling campaigns and laboratory analyses.

This material is based upon work supported under a National Science Foundation Graduate Research Fellowship and by SAHRA (Sustainability of semi-Arid Hydrology and Riparian Areas) under the STC Program of the National Science Foundation, Agreement No. EAR-9876800. Any opinions, findings, conclusions or recommendations expressed in this publication are those of the authors and do not necessarily reflect the views of the National Science Foundation.

DEDICATION

A mi amada esposa Angélica y a mis queridos padres, Ramón y Sylvia. Su amor, apoyo y compañía me ayudaron a completar este recorrido…

TABLE OF CONTENTS

LIST OF FIGURES 6
LIST OF TABLES 8
ABSTRACT 9
1 INTRODUCTION 10
2 METHODS 13
2.1 Site description 13
2.2 Hierarchical sampling campaign 15
2.3 Temperature as a tracer 16
2.4 Temperature surveys 22
2.5 Determination of direction and magnitude of flux 25
2.6 Uncertainty estimation 27
2.7 Statistical tests 28
2.8 Geostatistics 29
3 RESULTS 31
3.1 Vertical flux profiles 31
3.2 Temporal dependence of vertical fluxes 38
3.3 Seepage meter fluxes and Stallman's fluxes 45
3.4 Geostatistics 47
4 DISCUSSION 54
4.1 Vertical exchange, time since flood and stream discharge 54
4.2 Spatial structure of streambed fluxes 55
4.3 Implications 57
5 CONCLUSION 60
APENDIX A: MATLAB CODE TO APPLY STALLMAN'S ANALYTAL SOLUTION 62
APENDIX B: MATLAB CODE TO APPLY BOOTSTRAP CONFIDENCE INTERVAL ANALYIS TO FLUX DISTRIBUTIONS 72
REFERENCES 78

LIST OF FIGURES

Figure 1: Study site map 14

Figure 2: Schematic representation of the nested hierarchy 16

Figure 3: Example of a measured 24-hr temperature time series (symbols) and the sinusoidal fit to the measured data (lines) 19

Figure 4: Stallman's flux contour lines as a function of time lag ratio (t_ℓ / τ) and amplitude ratio ($\Delta T_s / \Delta T_w$) 21

Figure 5: Mean daily discharge at San Pedro River at Charleston, AZ 23

Figure 6: Schematic of temperature sensor set-up 25

Figure 7: Examples of the distribution types found 32

Figure 8: Median vertical flux profile for the 10 Km sampling extent and all sampling campaigns as a function of downstream distance 33

Figure 9: Median vertical flux profile for the 1 Km sampling extent and all sampling campaigns as a function of downstream distance 34

Figure 10: Median vertical flux profile for the 100 m sampling extent and all sampling campaigns as a function of downstream distance 35

Figure 11: Median vertical flux profile for the 40 m sampling extent and all sampling campaigns as a function of downstream distance 36

Figure 12: Median flux rate value for sites with upward flux for each sampling extent with respect to sampling campaign 39

Figure 13: Median flux rate value for sites with downward flux for each sampling extent with respect to sampling campaign 41

Figure 14: Median flux rate value for sites with upward flux at all extents with respect to sampling campaign 42

Figure 15: Median flux rate value for sites with downward flux at all extents with respect to sampling campaign 43

Figure 16: Median flux rate value for all sites and extents 44

LIST OF FIGURES - *Continued*

Figure 17: Correlation plot of Stallman's Flux versus measured fluxes using seepage meter 46

Figure 18: Semi-Variograms of the flux for the 10 Km sampling extent..... 49

Figure 19: Semi-Variograms of the flux for the 1 Km sampling extent..... 50

Figure 20: Semi-Variograms of the flux for the 100 m sampling extent..... 51

Figure 21: Semi-Variograms of the flux for the 40 m sampling extent..... 52

Figure 22: Correlation plot of average streamflow versus the months after flood for each sampling campaign 54

LIST OF TABLES

Table 1: Values (standard deviation) assigned to parameters used to solve Stallman's analytical solution. 20

Table 2: Number of consecutive 24hr temperature time series per sampling campaign and extent..... 24

Table 3: Median vertical flux (cm/s) by streambed type at the 100 m extent 37

Table 4: Median vertical flux (cm/s) by streambed type at the 40 m extent 37

Table 5: Flux change in the median upward flux rate between sampling campaigns for each sampling extent. 39

Table 6: Flux change in the median downward flux rate between sampling campaigns for each sampling extent. 40

Table 7: Flux change in the median upward flux rate between sampling campaigns for all sampling extents..... 42

Table 8: Flux change in the median downward flux rate between sampling campaigns for all sampling extents..... 43

Table 9: Flux change in the median flux rate between sampling campaigns for all sampling extents..... 44

Table 10: Semi-Variogram model indices for all extents and sampling campaigns..... 53

ABSTRACT

Precipitation patterns in semi-arid river systems of the southwestern U.S. make stream-aquifer exchanges an important source of water in perennial rivers. Nonetheless, the spatial and temporal evolution of surface and ground water interaction are not fully understood. This research utilizes diurnal temperature oscillations as a tracer of vertical water fluxes by applying Stallman's analytical solution to a series of temperature time series recorded in the stream and in the streambed of the San Pedro River. Temperature measurements were recorded at four spatial extents using a nested hierarchy during four different periods since last flood. Time since last flood did not affect vertical fluxes significantly, but fluxes exhibited spatial dependence at lengths of 6-24 m. Stream geomorphic features influenced the magnitude of vertical fluxes; runs were more downwelling than riffles. The data suggests that the spatial distribution of vertical fluxes becomes more homogeneous as time since last flood increases.

1 INTRODUCTION

Precipitation patterns in semi-arid river systems of the southwest U.S. make stream-aquifer exchanges an important source of water in perennial rivers [*Baillie et al.,* 2007; *Plummer et al.,* 2004; *Wahi et al.,* 2008]. Precipitation in the Sonoran Desert peaks bimodally in summer and winter with a distinct drought period in the spring months leading to the summer wet season. Summer precipitation is characterized by high intensity thunderstorms that are accompanied by increases in stream flow and an increased probability of flash flooding. These flash floods connect the stream with its hillslope and carry high concentrations of nutrients, organic matter and suspended solids into the stream [*Brooks and Lemon,* 2007; *Fisher and Minckley,* 1978].

In perennial river systems, streamflow after the floods and during the dry season is dominated by stream-aquifer interactions in the form of ground water discharge (baseflow) into the stream [*Pool and Coes,* 1999]. Stream-aquifer interactions and their effects on stream water quality have been the focus of numerous studies in semi-arid river systems of the Sonoran Desert [*Brooks and Lemon,* 2007; *Dent and Grimm,* 1999; *Dent et al.,* 2001; *Grimm et al.,* 1991; *Grimm,* 1987; *Holmes et al.,* 1994; *Jones et al.,* 1995b; *Valett et al.,* 1990; *Valett et al.,* 1994]. During baseflow periods, Fluorescence Index (FI) values indicate that the organic matter in streams switches from terrestrial sources during and after floods to aquatic sources as time since last flood increases [*Brooks and Lemon,* 2007]. This change is indicative of the hydrological disconnection between river and terrestrial ecosystems as well as the importance of stream-aquifer interactions in arid and semi-arid environments. In addition, these studies suggest that stream-aquifer

interactions and hyporheic zone nutrient cycling are important components controlling stream water composition. Research suggests that change in the direction of the vertical flux between surface and ground water induce changes in the chemical composition of surface and ground waters [*Dent et al.,* 2001; *Jones et al.,* 1995c; *Valett et al.,* 1994]. Furthermore, the direction of the vertical flux can determine whether a location of exchange acts as a source or sink of nutrients to the stream [*Dent et al.,* 2001; *Jones et al.,* 1995c; *Valett et al.,* 1994]. Moreover, the relationship between direction of exchange and its effects on surface and ground waters is space and time dependent [*Dent and Grimm,* 1999; *Dent et al.,* 2001; *Holmes et al.,* 1994]. All this suggests that in order to understand the processes controlling stream water composition throughout a flood succession cycle it is necessary to first understand the spatial and temporal evolution of surface and ground water interaction.

Diurnal air temperature fluctuations force diurnal temperature fluctuations in surface waters. These oscillations force continuous pulses of energy that propagate downward through saturated sediments. Therefore diurnal oscillations in temperature provide a natural tracer of water as it moves through a porous medium. Many researches have developed methods for analyzing how these energy pulses propagate and dissipate through streambed sediments to estimate magnitude and direction of water fluxes between surface and ground waters [*Becker et al.,* 2004; *Conant,* 2004; *Hatch et al.,* 2006; *Keery et al.,* 2007; *Silliman and Booth,* 1993; *Silliman et al.,* 1995; *Stallman,* 1965; *Stallman,* 1965; *Suzuki,* 1960]. *Anderson* [2005] has made a comprehensive review of the work done in this field.

This study addresses the following questions: (1) How does surface and groundwater vertical exchange vary in response to time after flooding and streamflow amount? (2) How does the spatial structure of streambed fluxes vary in response to time after flooding and streamflow amount?

2 METHODS

2.1 Site description

This study was conducted on the San Pedro River about 13 Km east of Sierra Vista, Arizona, USA (31°33'07" N, 110°08'19" W) between March 2006 and April 2007. The San Pedro River, a tributary of the Gila River, itself a tributary of the Colorado River, is a north-flowing trans-boundary river originating near the town of Cananea in the state of Sonora, Mexico and flowing into southeastern Arizona. The study site consists of four river reaches inside a 10 Km river stretch located in the San Pedro River National Conservation Area (SPRNCA) and centered at the intersection of Highway 90 with the river (Figure 1). The study site's drainage area ranges from 2,645 Km^2 to 3,034 Km^2 at the upstream and downstream ends of the 10 Km river stretch. Of the study site total drainage area 1,796 Km^2 lie in Mexico. The elevations at the upstream and downstream ends of the 10 Km river segment are 1242 m and 1218 m, respectively, while the maximum elevation within the drainage area is 2605 m.

According to *Hereford* [1993] and similar to other semi-arid river systems of the Sonoran Desert [*Dent et al.,* 2001], precipitation is bimodally distributed during the summer and winter months. The summer wet season generally starts mid-June and ends mid-October to early November. Precipitation in that period, commonly known as the Summer Monsoon, is characterized by high intensity and low duration rainfall caused by convective activity. The winter wet season generally starts early in December and ends late in March and is characterized by low intensity long duration storms. Flash floods are more common during the summer wet season but can also occur during the winter wet

season. Average annual precipitation based on 100 years of record from the Tombstone Precipitation Station is 35.3 cm at an elevation of 1405 m [*Pool and Coes,* 1999].

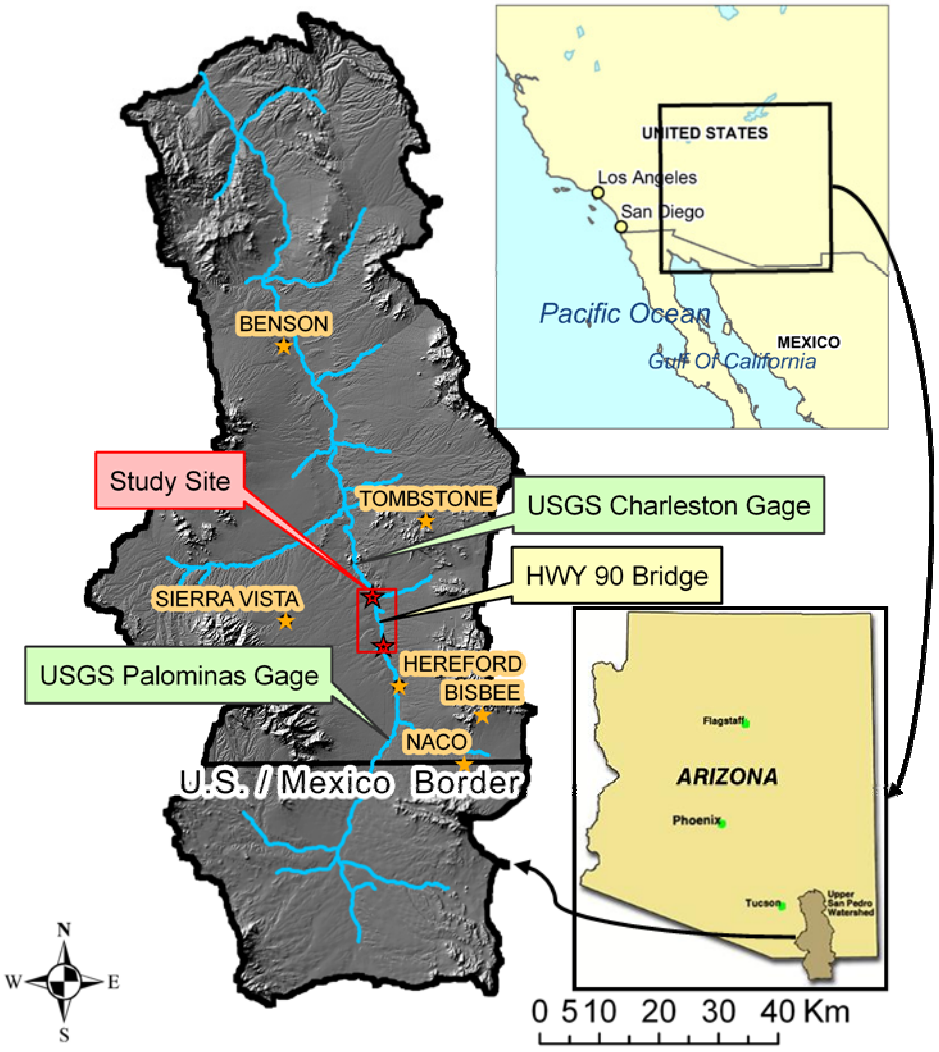

Figure 1: Study site map. The 10 Km study reach is bounded by the two red stars inside the red box.

During the study period (March 2006-April 2007), discharge measurements from the two nearest USGS streamflow stations (USGS Station 09470500, San Pedro River at Palominas, AZ, south of the study reach; and USGS Station 09471000 San Pedro River at

Charleston, AZ, north of the study reach) indicated that the 31 Km of river separating both stations were consistently gaining except for the period between July, 3 2006 and October 11, 2006. This time period coincides with the 2006 summer monsoon season. Water from shallow and deep aquifer systems maintains perennial flow in the study area, which supports a corridor of riparian vegetation, comprised mainly of phreatophytes, that is tens of meters wide [*Pool and Coes,* 1999]. The average winter and summer baseflow at the San Pedro River at Charleston, AZ, are 308.6 L^3/s and 82.1 L^3/s, respectively [*Pool and Coes,* 1999]. During our study, the uppermost 500 m of the study reach became dry during May 2006. This condition assured that water flowing into our study reaches during May 2006 came directly from the groundwater thus disconnecting the stream from any upstream influence.

2.2 Hierarchical sampling campaign

A nested hierarchy sampling design was applied for sample collection. Using this approach, river reaches are organized so that smaller river reaches are a subset of the preceding sampling extent (Figure 2). Four river reaches with longitudinal extents along the river of 40 m, 100 m, 1000 m and 10 Km were investigated. Each hierarchical level (extent) was associated with a sampling interval. Within each extent, sampling stations were set up at an associated sampling interval. The sampling extent and associated sampling intervals were: (1) 40 m extent at 1 m intervals, (2) 100 m extent at 2.5 m intervals, (3) 1000 m extent at 25 m intervals, and (4) 10 Km extent at 250 m intervals. The 100 m extent encompassed a run-riffle-run-riffle sequence while the 40 m extent

encompassed a run-riffle-run sequence. There were a total of 164 sampling stations. But, because of the nested hierarchy, some sampling stations coincided lowering the total to 145 sampling stations.

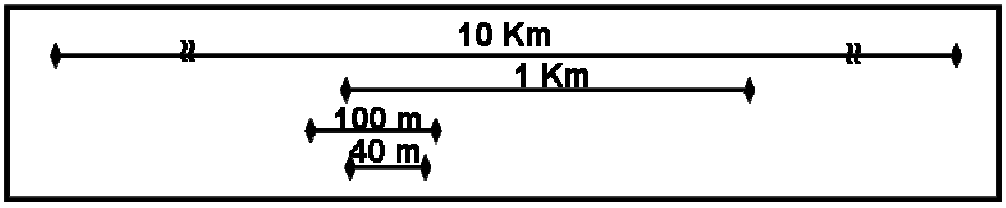

Figure 2: Schematic representation of the nested hierarchy. Each line represents a segment of a river reach.

At each sampling station, a 1.5 m long and 1.3 cm diameter segment of rebar was pounded in the center of the stream on March 4, 2006. The rebar served two purposes: first, it served as a sampling station marker; second, it served as a temperature sensor anchoring point. The rebar was left in place for the duration of the study. During the course of the Summer Monsoon floods of 2006, approximately 50 pieces of rebar were lost and were replaced on November 4, 2006.

2.3 Temperature as a tracer

Recent advances in temperature sensor design have made small and self logging temperature sensors readily available and inexpensive [*Johnson et al.,* 2005]. These sensors have enabled the use of temperature as an environmental tracer to: identify the direction of water exchange [*Silliman and Booth,* 1993]; quantify rates of exchange between surface and ground waters [*Conant,* 2004; *Keery et al.,* 2007; *Silliman et al.,*

1995]; and detect streamflow in ephemeral channels [*Blasch et al.,* 2005; *Constantz et al.,* 2002].

Stallman (1965) developed an analytical solution (eq. 2) to steady one-dimensional anisothermal flow of an incompressible fluid through a homogeneous porous medium with a sinusoidal surface temperature (eq. 1) that was originally approximated by Suzuki (1960).

$$k\frac{\partial^2 T}{\partial z^2} - qc_o\rho_o\frac{\partial T}{\partial z} = c\rho\frac{\partial T}{\partial t} \tag{1}$$

The analytical solution (eq. 2, 3 and 4) assumes: (1) sinusoidal temperature fluctuation with constant amplitude at the upper boundary (eq. 5), (2) a constant and uniform vertical flux rate, (3) all components of heat and fluid flow occur only vertically, and (4) the temperature of the interstitial water in the streambed sediments is the same as that of the sediment. The full derivation of this analytical solution can be found in Stallman, R (1965). The analytical solution is based on analysis of temperature time series at the surface and at depth to identify the reduction in the range of variation at depth (ΔT_S) relative to the range of variation at the surface waters (ΔT_w) and the time lag between the peaks of the two time series (t_ℓ) (Figure 3).

$$q = \frac{\left(b^2 - a^2\right)\times k}{\left(a \times c_o \times \rho_o\right)} \tag{2}$$

Where,

$$a = \frac{\log\left(\Delta T_s / \Delta T_w\right)}{z}$$

(3)

and,

$$b = \frac{2 \times \pi \times t_l}{\tau \times z} \tag{4}$$

$$T_{s,w}(t) = T_{ave_{s,w}} + \Delta T_{s,w} \times \sin\left(2\pi(t - t_{p_{s,w}})/\tau\right) \tag{5}$$

Where,

q=Water Flux at point z, taken positive in the upward direction (cm s^{-1})

ΔT_s=Range of temperature variation of sediment at depth z (°C) (Figure 3)

ΔT_w=Range of temperature variation of stream water (°C) (Figure 3)

z=Depth of sediment temperature measurement (cm) (Figure 6)

T_s =Temperature of sediment at time *t* (°C)

T_w =Temperature of water at time *t* (°C)

T_{ave}=Average temperature (°C)

t_{ps}=Time of peak of sediments (s) (Figure 3)

t_{pw}=Time of peak of water (s) (Figure 3)

$t_l = t_{ps} - t_{pw}$ =Time lag of temperature wave at depth z (s) (Figure 3)

τ =Period of oscillation of temperature in stream water (s)

t_p=Time of maximum temperature (s)

k=bulk heat conductivity of soil and water (cal sec^{-1} cm^{-1} $°C^{-1}$)

c_o=Water specific heat (cal g^{-1} $°C^{-1}$)

ρ_o=Water density (g cm^{-3})

c=Bulk specific heat (cal g^{-1} $°C^{-1}$)

ρ=Bulk density (g cm^{-3})

*Subscripts *s* and *w* refer to the parameter for sediment temperature and surface water temperature, respectively.

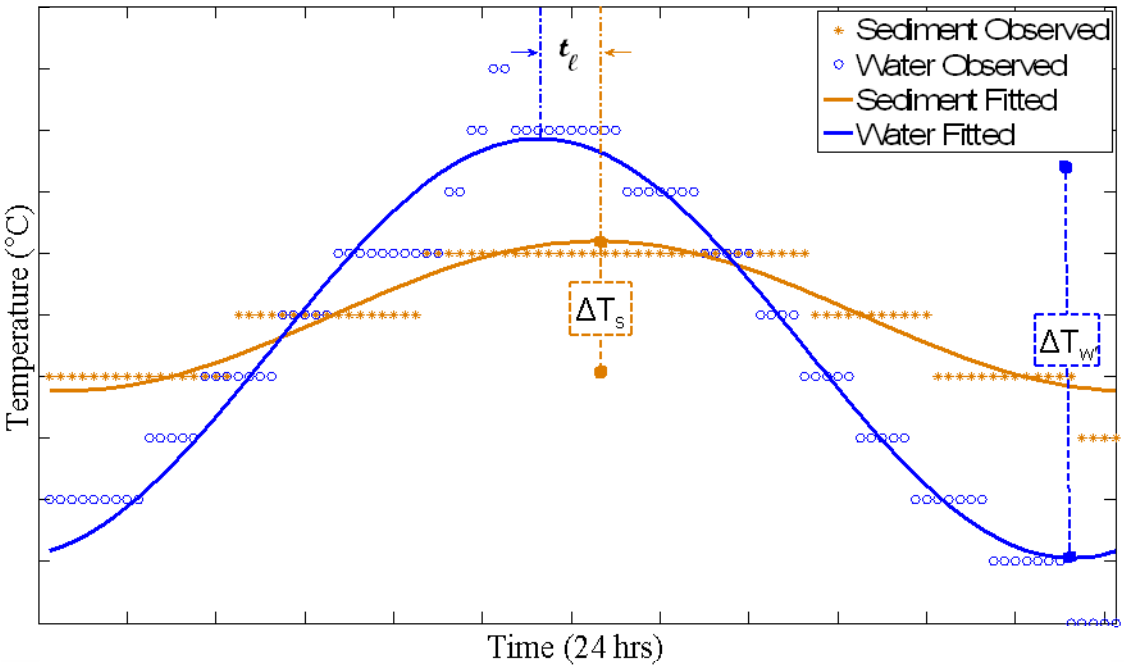

Figure 3: Example of a measured 24-hr temperature time series (symbols) and the sinusoidal fit to the measured data (lines). The vertical dashed lines with a box in the middle represent the range of temperature variation (**ΔT_s or ΔT_w**) while the vertical dot-dashed lines bounded by the arrows represent the time lag of the temperature wave at depth (**t_l**) as calculated from the sinusoidal fit. Note that the items are color coded (blue for the water column and brown for the sediments)

The values of the time lag ratio (t_ℓ/τ) and the amplitude ratio ($\Delta T_s/\Delta T_w$) of two sinusoidal wave functions are sufficient to yield a correct direction of the vertical flux if the assumptions underlying Stallman's solution are satisfied. The magnitude of the vertical flux is obtained when the depth of the sensor (z), thermal conductivity (k), fluid heat capacity and density are known. A two-dimensional parameter sensitivity analysis of $\Delta T_s/\Delta T_w$ and t_ℓ/τ (Figure 4) using fixed values of k and z parameters (Table 1) shows that the sensitivity of Stallman's solution to the input parameters depends on the input parameter values. In particular, the solution is more responsive to negative (downward)

and positive (upward) flux values close to zero. The response surface indicates that the maximum upward flux that can be calculated in the case studied here is approximately $1.7x10^{-3}$ cm/s, while the maximum downward flux approaches infinity.

Stallman's analytical solution relies on identifying and calculating amplitude reduction and phase shift between two diurnal temperature time series. Therefore, the determination of magnitude and direction of the vertical flux using Stallman's solution is highly dependent on the ability to record temperature differences as precisely as possible. Stallman (1965) suggested that his analytical solution would work best in conditions of low heat conductivity, large daily temperature oscillation at the surface and careful measurements of temperature fluctuations.

Table 1: Values (standard deviation) assigned to parameters used to solve Stallman's analytical solution.

Parameter	Value	Units	Source
Temp time series	measured(0.19^{1})	°C	manufacturer
ΔTs	variable(variable)	°C	sinusoidal fit
ΔTs	variable(variable)	°C	sinusoidal fit
t_{ps}	variable(variable)	sec	sinusoidal fit
t_{pw}	variable(variable)	sec	sinusoidal fit
τ	86400	sec	assumed
Depth (z)	10 (1.28) cm	cm	assumed
Thermal conductivity (k)	5.682 (0.598) x 10^{-3}	cal sec^{-1} cm^{-1} $°C^{-1}$	[*Coes and Pool,* 2005]

[1]Estimated from the Dallas Semiconductor *i*button temperature confidence interval at 99% significance which was the largest between the two sensors used.

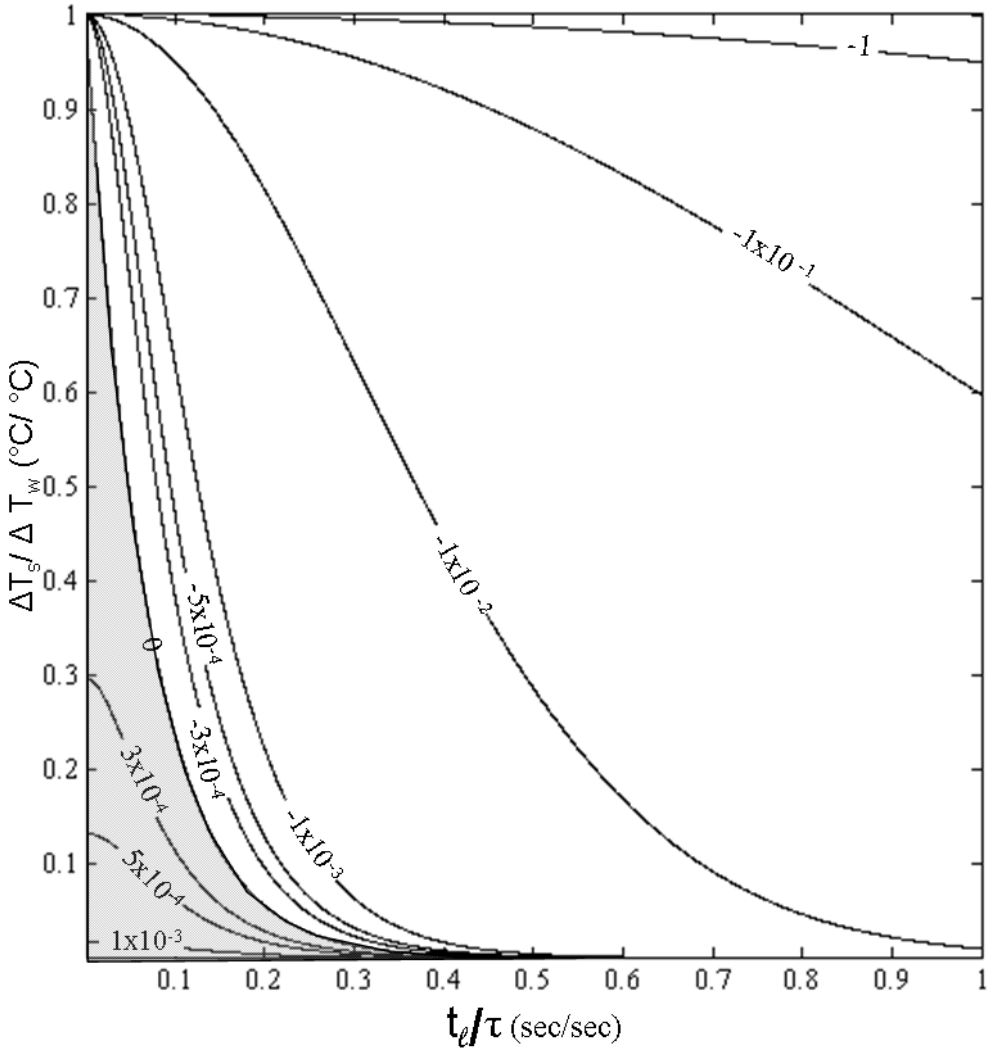

Figure 4: Stallman's flux contour lines as a function of time lag ratio (t_ℓ / τ) and amplitude ratio ($\Delta T_s / \Delta T_w$). Flux values are based on a thermal conductivity value of ($k = 5.68 \times 10^{-3}$ cal sec^{-1} cm^{-1} $°C^{-1}$) and depth value of ($z = 10$ cm). Note that upward fluxes occur at the shaded region of the parameter space. Fluxes contour units are in cm/s.

One of the main limitations with Stallman's analytical solution is that as upward fluxes increase, heat pulse propagation through streambed sediments diminishes. At depth and independent of flux directionality, heat pulse propagation is controlled by advective, diffusive and dispersive processes. The directionality of the flux controls the

source of the heat that will be propagated by advection. At daily timescales, groundwater temperatures can be assumed constant and when an upward flux is sufficiently high it will prevent diurnal heat pulses from propagating from the surface. These locations will experience a nearly constant temperature time series making it difficult or impossible to correctly identify the timing of the peak of the sediment temperature (many times non-existent) and thus the t_ℓ parameter. It is expected that under high upward fluxes Stallman's analytical solution will fail to yield a correct answer because heat pulses can not propagate downward thought streambed sediments. Therefore, Stallman's solution is best suited to quantify downward fluxes with a limited ability to quantify upward fluxes. Nevertheless, due to the nature of heat pulse propagation, the direction of the vertical flux and a lower bound estimate of the flux can still be assessed. At locations with a nearly constant sediment temperature profile only a lower bound estimate of the upward flux is possible based on the maximum upward flux ($1.7x10^{-3}$ cm/s) obtained from the parameter perturbation analysis.

2.4 Temperature surveys

Temperature surveys were done during a two-week period for all sampling stations centered on the four campaign dates: March 18, 2006, May 21, 2006, November 18, 2006 and April 21, 2007. The number of months since the last flood event occurred for each sampling campaign was: 6.3, 8.4, 2.2 and 7.3, respectively. Mean daily discharge values (± one standard deviation) for each two week sampling campaign were: 294.9±5.8 L^3/s, 61.4±15.2 L^3/s, 391.1±8.8 L^3/s, and 259.5±22.5 L^3/s, respectively (Figure 5). The state of the deciduous riparian vegetation during each sampling campaign was: prior to leaf

out; after leaf out; during leaf fall; and during leaf out, respectively. The temperature surveys of the 10 Km and 1000 m extents were done the week before the sampling campaign, while the temperature surveys of the 100 m and 40 m reaches were done the week after the sampling campaign. Two self-contained temperature logging sensors were placed at each sampling station. The first was placed in the sediments 10 cm below the top of the stream-streambed interface while the second was placed in the overlying stream water column (Figure 6). The sensors were programmed to collect data synchronously at 15 minute intervals for the numbers of days listed on table 2 at each sampling location.

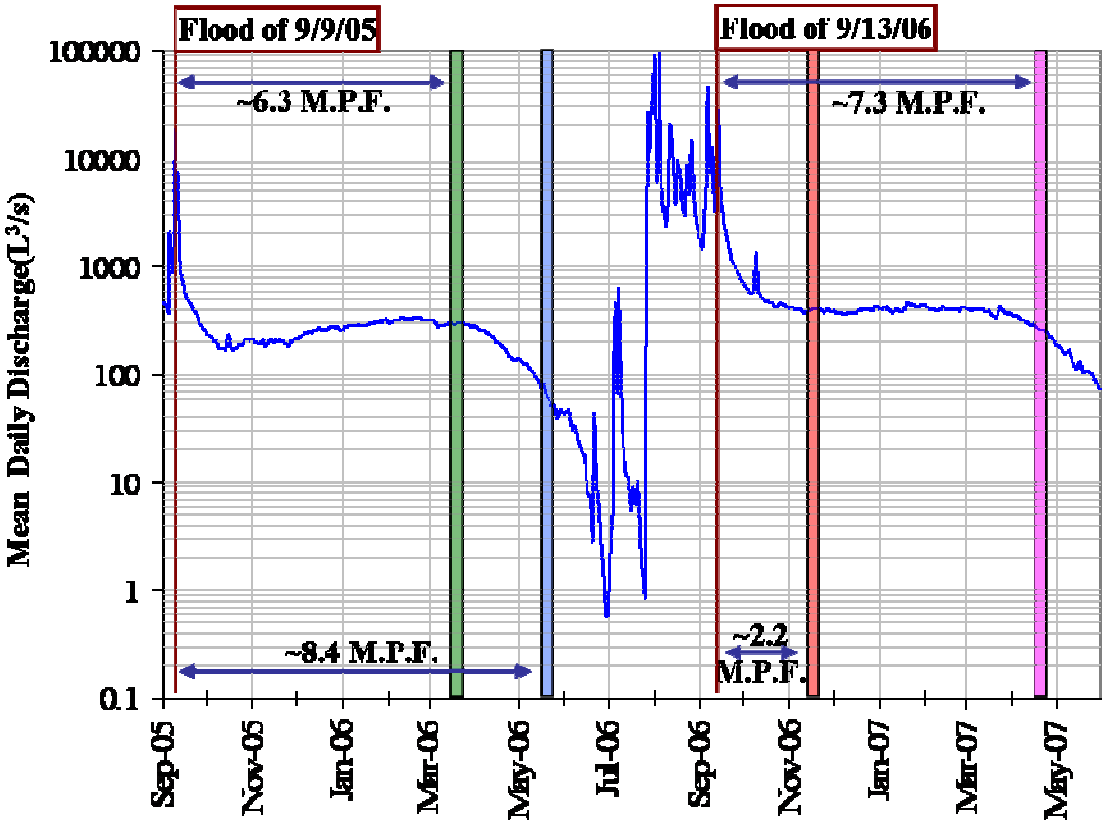

Figure 5: Mean daily discharge at San Pedro River at Charleston, AZ (USGS 09471000). Red vertical line shows last floods of the 2005 and 2006 summer monsoon seasons. Colored vertical

rectangles indicate timing of the sampling campaigns (green for March 2006, blue for May 2006, red for November 2006 and pink for April 2007).

Due to equipment malfunctions and sensor loss, the number of available temperature sensors decreased during the progress of the field campaigns. After the first sampling campaign it was noted that surface water temperatures did not vary significantly between sampling stations. Therefore, the available sensors were primarily allocated to measure sediment temperature and the remaining sensors were divided to measure surface water temperatures. In locations where a sensor failed or no surface water sensor was deployed, surface water temperature measurements made at the nearest surface water temperature measurement site were used.

Table 2: Number of consecutive 24hr temperature time series per sampling campaign and extent

Sampling Extent	10 Km	1 Km	100 m	40 m
Mar-08	7	7	6	6
May-08	6	6	9	9
Nov-08	6	6	6	6
Apr-08	6	6	6	6

Two types of temperature sensors were used in this study. One was the Dallas Semiconductor's *i*Button DS1921G-F5 with a temperature accuracy of ± 1 C° (at 99% significance). The other was the Onset Computer Corporation StowAway Tidbit with a temperature accuracy of ± 0.2 C° (at 99% significance). According to the manufacturer, the *i*Button is water resistant for 1 day at 1 m depth and not water proof. Therefore, a

water proofing system for the *i*Buttons was devised by encasing them in a threaded 19.05 mm pipe cap and pipe plug set. The Tidbit is encased in an epoxy resin; therefore no additional water proofing was necessary. After the two week deployment for each campaign, the data were downloaded from the sensors using the manufacturer-supplied equipment and stored in a database.

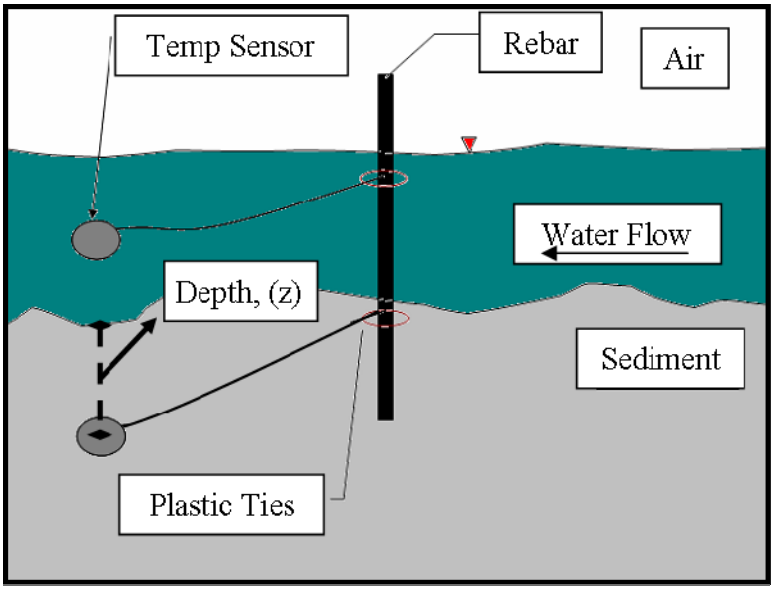

Figure 6: Schematic of temperature sensor set-up. Two temperature tensors were anchored to a 1.5 m long piece of steel rebar at the thalweg of the stream. The first was placed in the sediments 10 cm bellow the top of the stream-streambed interface while the second was placed in the overlying stream water column.

2.5 Determination of direction and magnitude of flux

Temperature was used to determine the direction of stream-aquifer exchange at all sampling extents. MATLAB® 7.5 (Natick, MA), a technical computing environment, was used to automate the process of applying Stallman's analytical solution. Stallman's analytical solution requires the identification of the range of variation and time of peak

for both the sediment and the surface water. To identify these parameters, the temperature time-series was divided into successive 24-hour time series. Each 24-hour temperature time series corresponded to one day of the temperature sensor deployment. After dividing, a sinusoidal equation (eq. 5) was fitted, using the MATLAB® "fit" function, to each 24 hour time series to estimate the range of variation of temperature (ΔT_s, ΔT_w) (Figure 3), the timing of the peak (Figure 3) and a 95% confidence interval for each estimated parameter.

After the sinusoidal function was fitted for the sediment and surface water, the time lag (t_ℓ) was determined by subtracting the timing of the peak of the surface water from that of the sediments. It was expected that this process would yield only positive t_ℓ values so that $0 \leq t_\ell < 24$ hrs. It was assumed that a negative t_ℓ value indicated that the observed peak time of the sediment temperature for any 24-hr time series belonged to the previous 24-hr time series. If the process of finding the t_ℓ values created a negative value and if this value was greater than 0.5 hrs then 24 hrs were added to the negative t_ℓ value. It was also assumed that any t_ℓ value that satisfied the inequality $-0.5 < t_\ell < 0.5$ hrs (this corresponds to two times our temporal sampling interval) was equal to zero. This process was repeated for each sampling location for both the sediment and surface water to obtain seven estimates of the ΔT_s, ΔT_w and t_ℓ parameters. If any estimate of ΔT_s obtained from the sinusoidal fitting process was less than or equal to 0.75 °C (1.5 times the maximum temperature resolution of the sensors) it was assumed that the sediment temperature profiles had a "nearly" constant temperature time series. In this case the flux calculation was bypassed and an upward flux of 1.7×10^{-3} cm/s was assigned for that 24-hr time

period. Otherwise, each set of three parameters obtained every 24 hours together with the period of oscillation (Table 1), depth of measurement (Table 1), and an estimate of the thermal conductivity (Table 1) were fed into Stallman's analytical solution to obtain an estimate of the flux.

2.6 Uncertainty estimation

To determine the uncertainty of the flux estimate the uncertainties of the temperature time series and the parameters (ΔT_s, ΔT_w, t_{ps}, t_{pw}, z, and k) were propagated using a numerical approach. For this approach, the temperature time series and parameter uncertainties were assumed to be normally distributed. The calculation of the flux was iterated 150 times selecting parameters, values from a normal distribution at each location and 24-hr period. At every iteration, each value of the 24-hr temperature time series and parameter values were randomly sampled from a normal distribution with mean and standard deviation listed in Table 1. The mean and standard deviation of ΔT_s, ΔT_w, t_{ps}, t_{pw} were estimated from the 95% confidence intervals of the sinusoidal fit process. The output of this process was a distribution of flux values for which a median and 95% confidence interval were estimated using a bootstrap method [*Efron and Tibshirani,* 1986].

Due to the highly heterogeneous nature of the distributions coupled with extreme values present in some distributions, the median value of vertical flux was chosen as a measure (estimator) of centrality [*Bonett and Price,* 2002]. Choosing the median flux rate posed the challenge of estimating the uncertainty around the median. To overcome

this problem, the bootstrap methodology described in [*Efron and Tibshirani,* 1986] was used to estimate the uncertainty of the median flux rate at all sampling sites and times.

To estimate the uncertainty around the median flux value using bootstrapping, 10,000 sample groups of size n were obtained by sampling with replacement from the distribution of fluxes, where n is the size of the distribution sampled. The median was calculated for each sample group (1, 2, 3, 4, …, 10000) of size n. This approach generates a distribution of median values of size equal to 10,000. The distribution of median values is then sorted in ascending order. The 2.5^{th} and 97.5^{th} percentile values are used as the upper and lower bounds of the 95% percent confidence interval for the median while the midpoint (average) between two percentile values is used as the estimate of the median. This procedure is conducted by using the MATLAB®'s "bootci" function.

2.7 Statistical tests

To evaluate if vertical fluxes are affected by time since last flood a non-parametric paired Wilcoxon two-sided signed rank test (α=0.05) was applied to all possible pairs of sampling campaigns. This test requires that the distributions have the same length and that the data is paired in some way. To satisfy this requirement, the data points on each distribution of vertical fluxes were paired using the downstream distance value of each sampling location. Between sampling campaigns not all sampling locations could be paired due to sensor loss or failure. Therefore, a subset of each sampling campaign distribution of fluxes was used for the test. The campaign pairs tested were: March 2006 with May 2006, March 2006 with November 2006, March 2006 with April 2007, May

2006 with November 2006, May 2006 with April 2007, and November 2006 with April 2007.

The estimated flux values were summarized statistically by grouping the data into sets based on the temporal and spatial sampling design. The first two sets took the entire sample population and divided it into upwelling and downwelling for each extent and sampling campaign. The second two groups divided the total sample population into upward and downward fluxes but merged data from all sampling extents for a given field sampling campaign. The final set was created by merging data from all sampling extents regardless of flux direction for every sampling campaign.

After each set was created, the median and 95% confidence intervals were determined using the bootstrap methodology already described. To test if the median flux rate values between each successive sampling campaign were equal, a non-parametric Wilcoxon two-sided rank sum test (Mann-Whitney U-test) with α=0.05 (95% significance) was applied to all possible pairs of sampling campaigns. The pairs tested were: March 2006 with May 2006, March 2006 with November 2006, March 2006 with April 2007, May 2006 with November 2006, May 2006 with April 2007, and November 2006 with April 2007.

2.8 Geostatistics

Semi-variograms were created to test if vertical flux displayed spatial dependence longitudinally in the stream. Semi-variograms plot half of the average, squared difference between a pair of points against a separation (lag) distance [*Rossi et al.,* 1992]. MATLAB® was used to create a routine that would manually calculate and generate

semi-variograms plots as described in [*Rossi et al.,* 1992]. The minimum lag distance was set equal to the sampling interval for each sampling extent while the maximum lag was set to 30% of the sampling extent.

If semi-variance showed correlation with lag distance either a linear or spherical semi-variogram model was fitted manually. The manual fitting process used the coefficient of determination (R^2), the correlation slope (CS) between observed and modeled semi-variance to find a best fit model. The non-linear spherical semi-variogram model is given in equations 6 and 7.

If $h < A_0$,

$$\gamma (h) = C_0 + (S - C_0) \times (1.5 \times (h/A_0) - 0.5 \times (h/A_0)^3), \quad (6)$$

If $h \geq A_0$,

$$\gamma (h) = S \quad (7)$$

Where, $\gamma (h)$ is the semi-variance at lag h, C_0 is the nugget variance, S is the sill variance, A_0 is the range distance, and h is lag distance.

3 RESULTS

3.1 Vertical flux profiles

During the study period, the highest daily surface water temperature oscillation observed was 9 °C during the sampling campaign of May 2006. The diurnal surface water temperature oscillations for March 2006, November 2006 and April 2007 were all ~6 °C. The results of the uncertainty propagation show that the flux distributions among sampling sites and times do not follow a single distribution (Figure 7). These results support the decision to apply a bootstrap analysis to estimate confidence intervals around the median.

After applying Stallman's analytical solution and a bootstrap analysis, it is evident that vertical fluxes are highly variable in time and space (Figures 8, 9, 10, and 11). Changes in magnitude and direction of the vertical flux occur at spatial intervals of 1m and temporal intervals of 2.1 months. The vertical flux coefficient of variation for all sites in each sampling campaign was -177.10, -8.09, -124.89 and -15.15 for March 2006, May 2006, November 2006, and April 2007, respectively. Most of the estimated flux values fall between 1.7×10^{-3} cm/s and -1.5×10^{-3} cm/s (negative values indicate downward fluxes). Locations with an upward flux of 1.7×10^{-3} cm/s represent sites of nearly constant sediment temperature where a lower bound estimate of the upward flux was assigned. The magnitude of the uncertainty around the median is one or more orders of magnitude less than the median flux for most estimates. For most sample locations, the upper and lower error bars show are a single horizontal line, showing that the uncertainties of the

parameters translate to small uncertainties in the estimated fluxes (Figures 8, 9, 10, and 11).

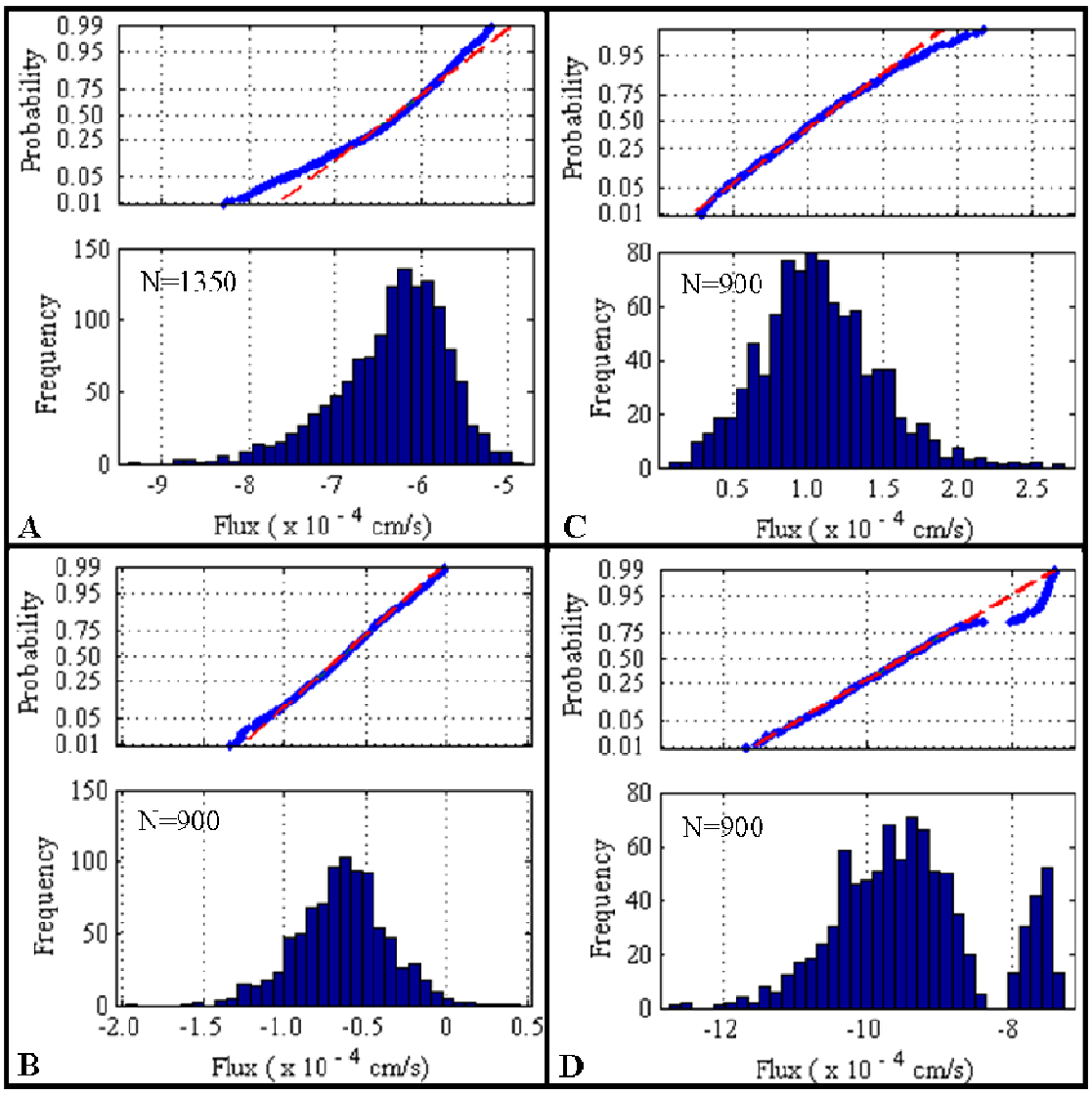

Figure 7: Examples of the distribution types found. On each pane, the upper graph represent a normal probability plot and the lower a histogram of the data plotted against flux (x axis). Note that positive flux values indicate upward flux while negative flux values indicated downward flux. On the normal probability plot the blue dots are data while the red line is a normally distributed line. If the blue line follows the red line it could be argued that the data is normally distributed. A) A negatively skewed dataset from May 2006 sampling campaign located at 3990 m from origin. B) A normally distributed dataset from April 2007 sampling campaign located at 500 m from origin. C) A positively skewed dataset from April 2007 dataset located at 7750 m from origin. D) A bimodally distributed dataset from March 2006 sampling campaign located at 4675 m from origin.

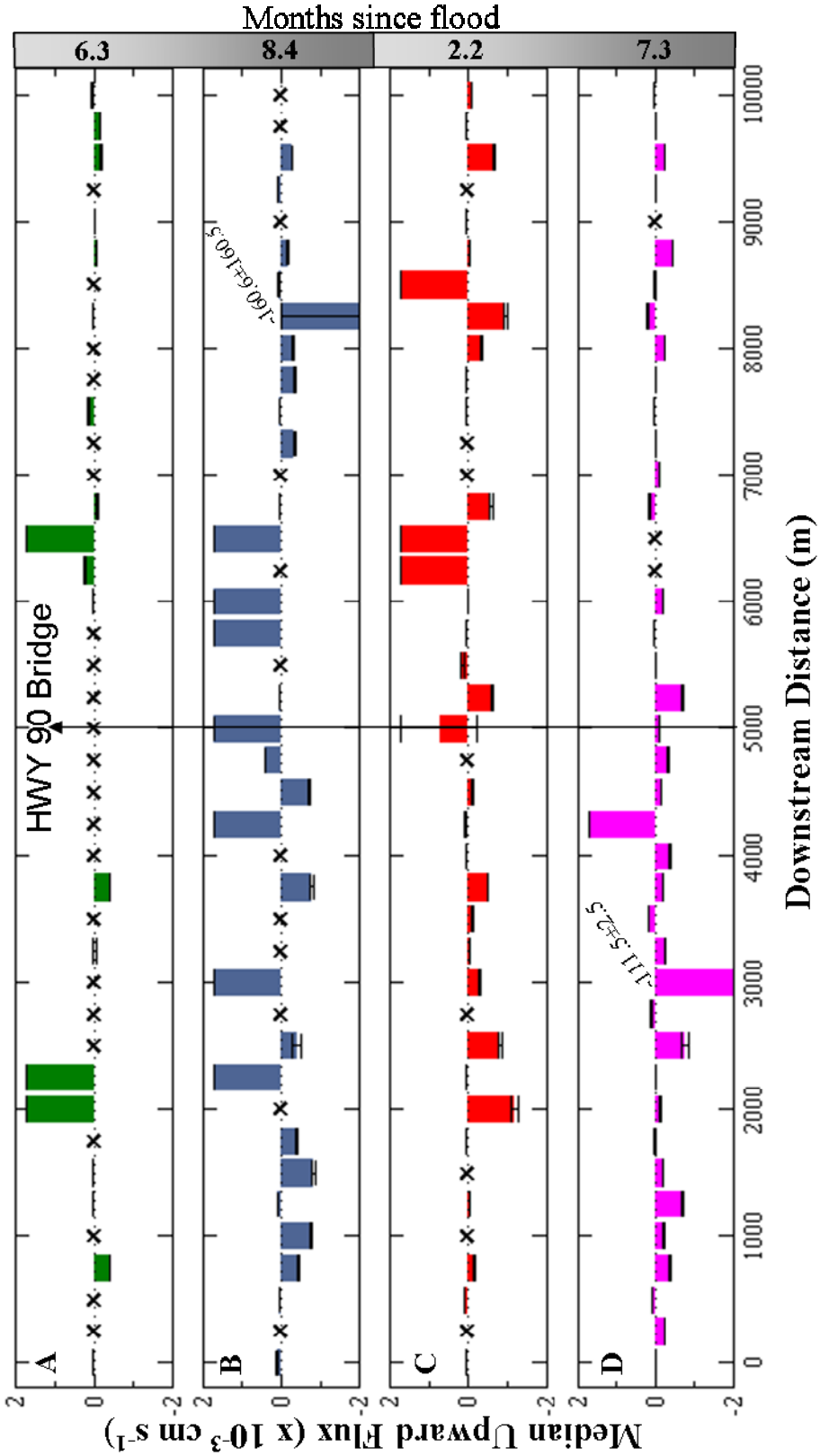

Figure 8: Median vertical flux profile for the 10 Km sampling extent and all sampling campaigns as a function of downstream distance. The secondary y-axis shows months since last flood. Bars indicate the estimate of median flux rate; the error bars indicate the 95% confidence intervals based on bootstrap analysis. The **x** symbols indicate no data while the pane letter and color indicate the different sampling campaigns: A) green for March 2006, B) blue for May 2006, C) red for November 2006 and D) pink for April 2007). Note that negative fluxes indicate downward flux or a losing point.

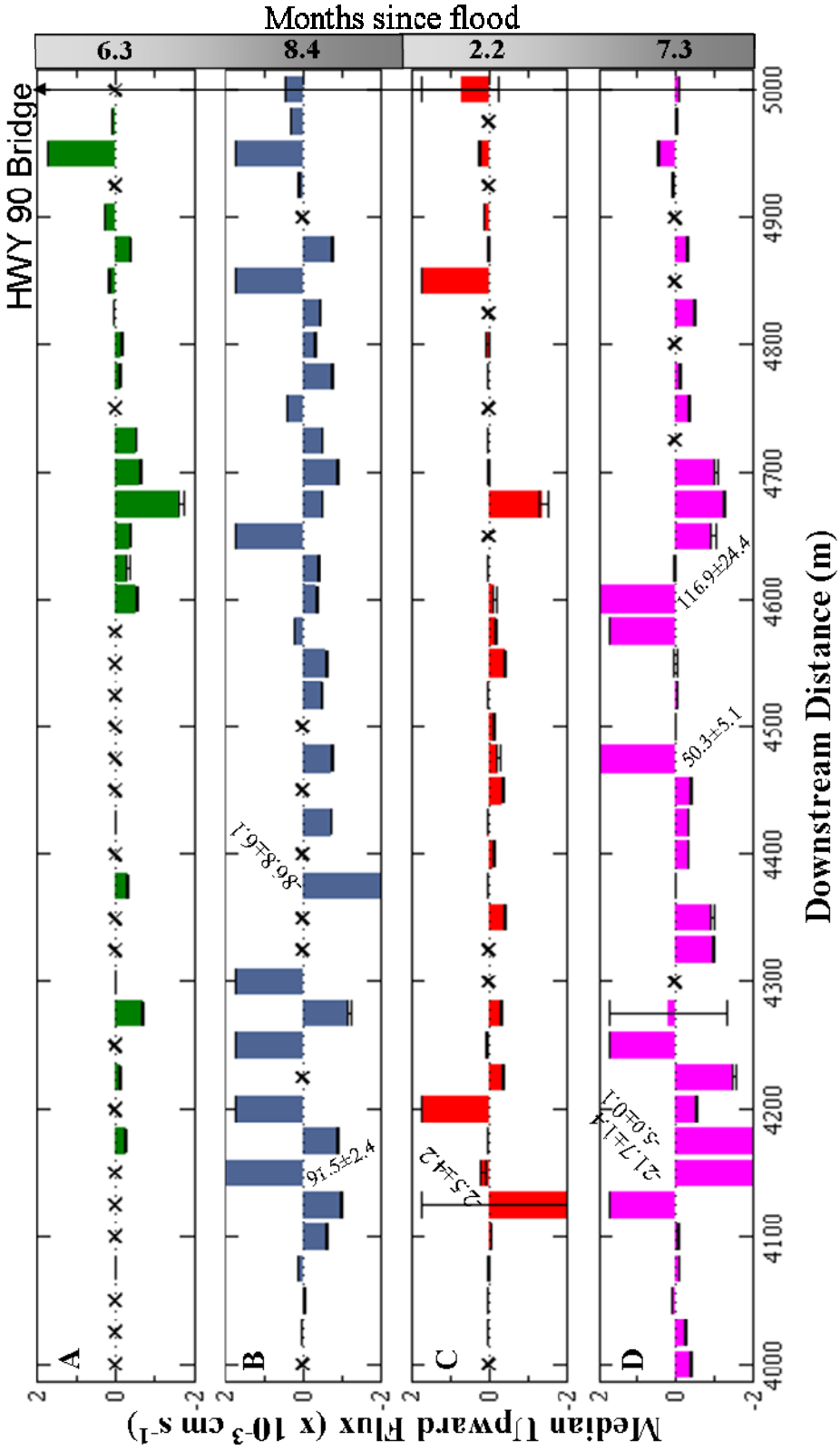

Figure 9: Median vertical flux profile for the 1 Km sampling extent and all sampling campaigns as a function of downstream distance. The secondary y-axis shows months since last flood. Bars indicate the estimate of median flux rate; the error bars indicate the 95% confidence intervals based on bootstrap analysis. The **x** symbols indicate no data while the pane letter and color indicate the different sampling campaigns: A) green for March 2006, B) blue for May 2006, C) red for November 2006 and D) pink for April 2007). Note that negative fluxes indicate downward flux or a losing point.

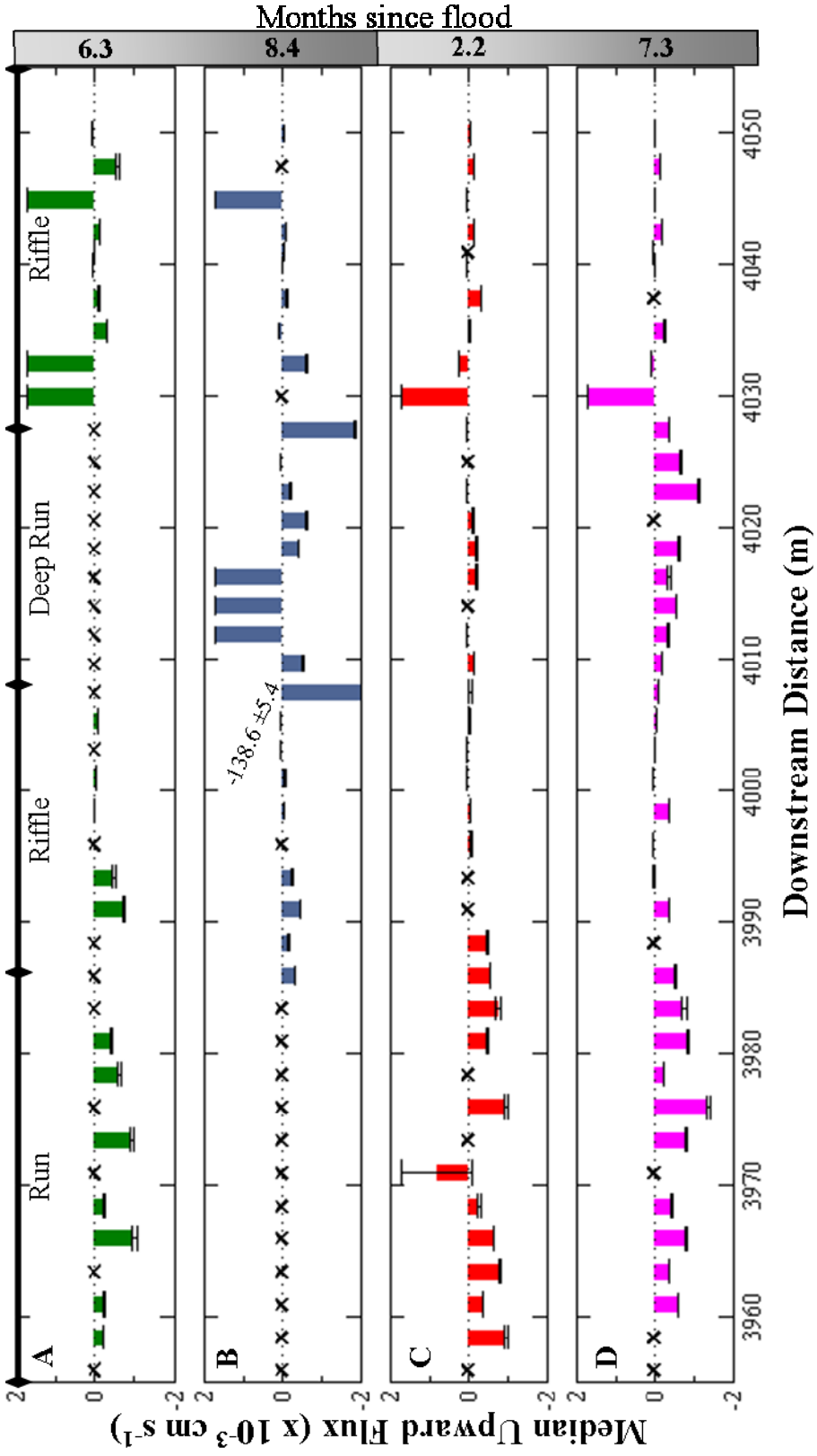

Figure 10: Median vertical flux profile for the 100 m sampling extent and all sampling campaigns as a function of downstream distance. The secondary y-axis shows months since last flood. Bars indicate the estimate of median flux rate; the error bars indicate the 95% confidence intervals based on bootstrap analysis. The **x** symbols indicate no data while the pane letter and color indicate the different sampling campaigns: A) green for March 2006, B) blue for May 2006, C) red for November 2006 and D) pink for April 2007). Note that negative fluxes indicate downward flux or a losing point. Also, on the upper margin the extent of the run, riffle, and pool sequence.

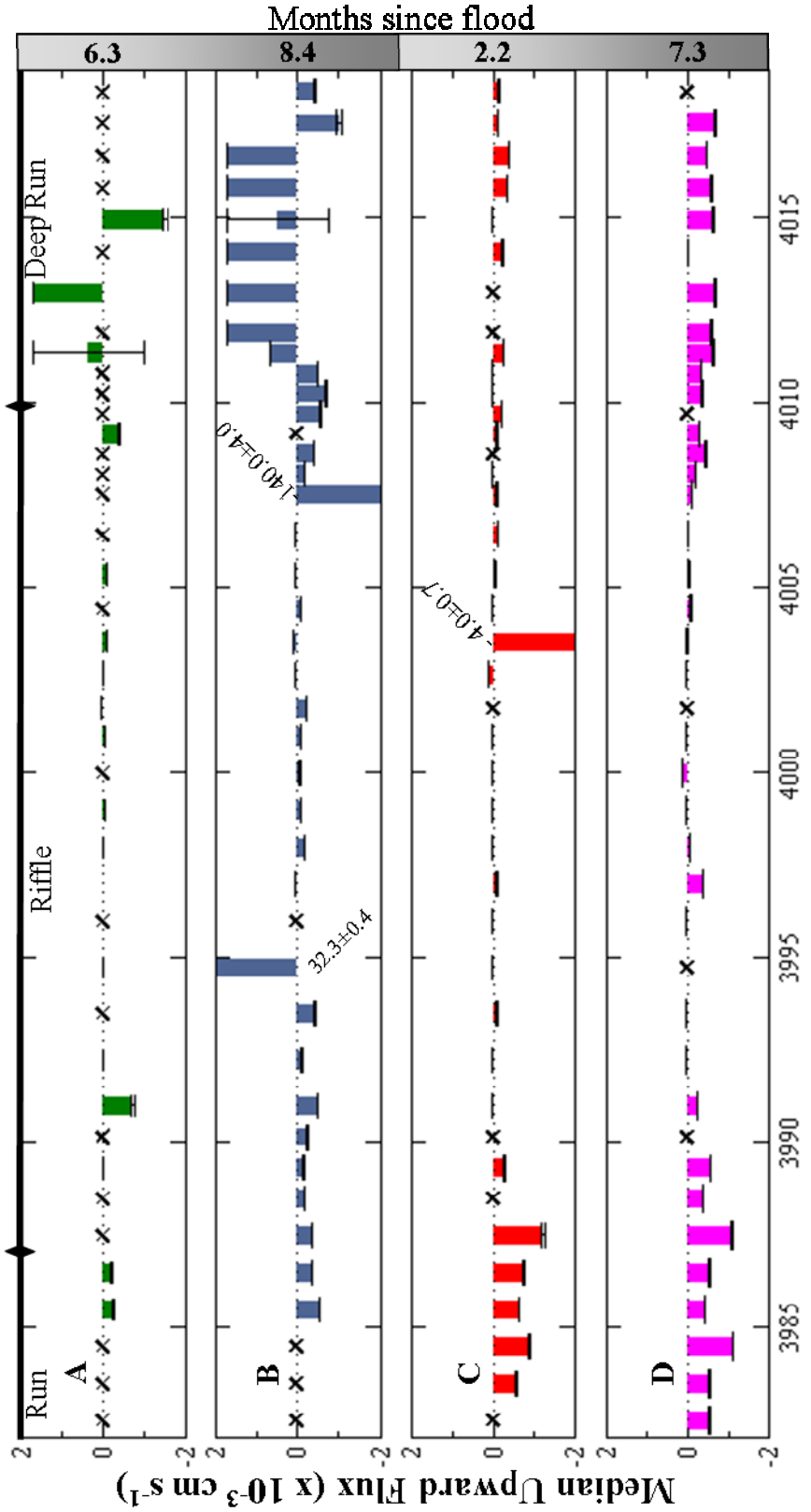

Figure 11: Median vertical flux profile for the 40 m sampling extent and all sampling campaigns as a function of downstream distance. The secondary y-axis shows months since last flood. Bars indicate the estimate of median flux rate; the error bars indicate the 95% confidence intervals based on bootstrap analysis. The **x** symbols indicate no data while the pane letter and color indicate the different sampling campaigns: A) green for March 2006, B) blue for May 2006, C) red for November 2006 and D) pink for April 2007). Note that negative fluxes indicate downward flux or a losing point. Also, on the upper margin the extent of the run, riffle, and pool sequence.

The upper boundary of Figures 10 and 11 includes a qualitative description of the streambed type (riffle, pool, run) as identified during the last temperature sensor deployment; no significant change in streambed type occurred over the study. At the 100 m and 40 m extent, median vertical flux rates at runs are an order of magnitude higher when compared to vertical fluxes at riffles (Table 3 and 4). At the 100 m extent during the sampling campaigns of March 2006, November 2006, and April 2007 a non-parametric Wilcoxon rank sum test (α=0.05) indicates that the median vertical flux rate between run and riffles is statistically different. The same test revealed that at the 40 m extent the median vertical flux rate between run and riffles was statistically different only for the April 2007 sampling campaign.

Table 3: Median vertical flux (cm/s) by streambed type at the 100 m extent

Type	Mar†	May	Nov†	Apr†
Run	-4.36E-04	-2.86E-04	-2.90E-04	-5.91E-04
Riffle	-5.25E-05	-8.94E-05	-6.02E-05	-2.63E-05

† Median flux rate magnitude between streambed type (i.e. run vs. riffle) at this sampling campaign are statistically different to a 95% significance level based on a non-parametric Wilcoxon rank sum test. Note that negative fluxes indicate downward flux or a losing point.

Table 4: Median vertical flux (cm/s) by streambed type at the 40 m extent

Type	Mar	May	Nov	Apr†
Run	-3.93E-04	-1.69E-04	-2.04E-04	-5.38E-04
Riffle	-2.15E-05	-1.12E-04	5.42E-06	-4.76E-05

† Median flux rate magnitude between streambed type (i.e. run vs. riffle) at this sampling campaign are statistically different to a 95% significance level based on a non-parametric Wilcoxon rank sum test. Note that negative fluxes indicate downward flux or a losing point.

3.2 Temporal dependence of vertical fluxes

To test if vertical fluxes exhibit temporal dependence, a series of non-parametric statistical test was applied to the entire dataset and subsets of the dataset based on the flux direction and sampling design. The paired non-parametric Wilcoxon two-sided signed rank test (α=0.05) showed that the difference of vertical fluxes among all possible combinations of sampling campaigns at each scale are symmetric with zero median with the exception of: March 2006 and November 2007 for the 1 Km extent, and November 2006 and April 2007 for the 100 m extent. These results suggest that the distribution of vertical fluxes when compared as a whole do not exhibit temporal dependence.

To better understand if any temporal pattern is present in the data, the dataset values were summarized statistically. Calculating the median flux rate for sites with upward fluxes in each extent and time highlights how variable the median upward flux is across sampling extents and time (Figure 12). Overall, there is a clear difference in the median upward fluxes before the summer floods of 2006 (May 2006) and after the summer floods of 2006 (November 2006 and April 2007) (Figure 12). Median upward fluxes decrease after the sampling campaign of May 2006. Analysis of this group shows that the median upward flux rate for the 10 Km, 1 Km, 100 m and 40 m extents (first, second, third and fourth bar in the group, respectively): (1) increases from March 2006 to May 2006, and (2) decreases from May 2006 to November 2006 (Table 5). A Wilcoxon rank sum test (α=0.05) suggests that: 1) the median upward flux rate between March 2006 and May 2006, May 2006 and November 2006, November 2006 and April 2007, and May 2006 and April 2007 were different for the 1 Km extents, and 2) the median upward flux rate

between March 2006 and May 2006, May 2006 and November 2007, and May 2006 and April 2007 were different for the 40 m extents. As opposed to the paired Wilcoxon two-sided rank test, this test suggest that time since last flood significantly influences upward fluxes at some sampling extents and times.

Table 5: Flux change in the median upward flux rate between sampling campaigns for each sampling extent.

Extent	Mar-May	May-Nov	Nov-Apr	Mar-Nov	Mar-Apr	May-Apr
10 Km	7.5E-04	-8.2E-04	-2.7E-06	-7.0E-05	-7.2E-05	-8.2E-04†
1 Km	8.7E-04†	-9.3E-04†	8.3E-04†	-5.2E-05	7.8E-04	-9.3E-05
100 m	1.4E-05	-7.3E-04	-9.7E-05	-7.2E-04	-8.2E-04	-8.3E-04
40 m	4.4E-04†	-8.5E-04†	5.3E-06	-4.1E-04	-4.1E-04	-8.4E-04†

† Median flux rate magnitudes between sampling campaign are statistically different at a 95% significance level based on a non-parametric Wilcoxon rank sum test.

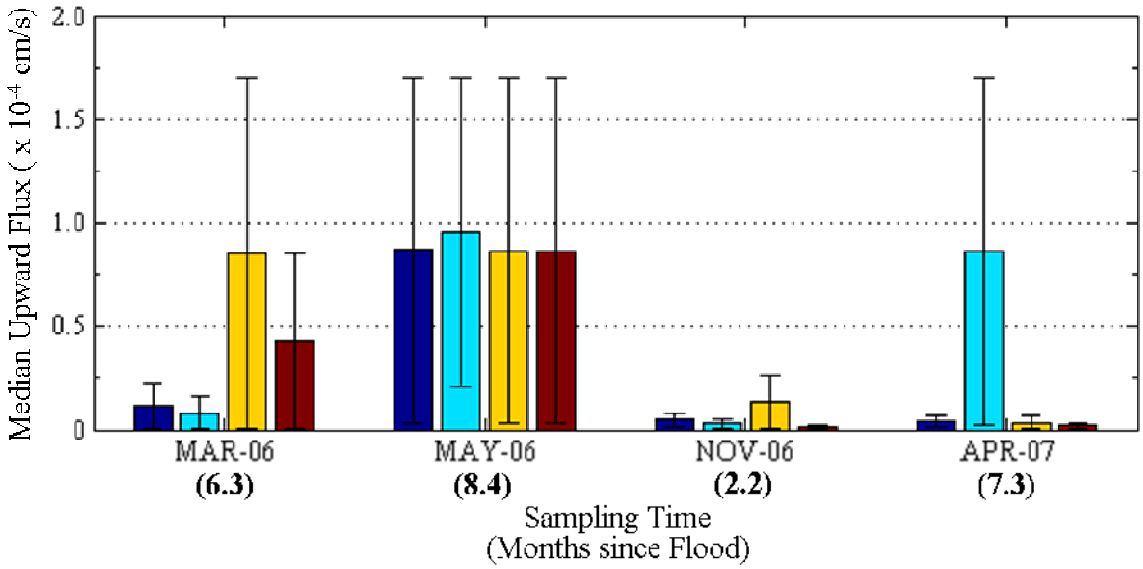

Figure 12: Median flux rate value for sites with upward flux for each sampling extent with respect to sampling campaign. From left to right the 10 Km, 1 Km, 100 m and 40 m extents are first (blue), second (cyan), third (yellow) and forth (brown) bar respectively. Note that the color pattern repeats for each sampling campaign. Error bars indicate the 95% confidence intervals based on a bootstrap analysis.

Analyzing the median flux rate for sites with downward fluxes in each extent and time indicates that downward fluxes are less variable than upward fluxes across sampling extent and time (Figure 13). Analysis of this group shows that no single trend is present at all extents (Table 6). The median downward flux rate for the 10 Km and 1 Km extents (first and second bar in each group respectively) (1) increases from March 2006 to May 2006, and (2) decreases from May 2006 to November 2006 (Table 6). A Wilcoxon rank sum test (α=0.05) shows that: 1) the median downward flux rate between March 2006 and May 2006, and May 2006 and April 2007 for the 10 Km extent were different, and 2) the median downward flux rate between March 2006 and May 2006, and May 2006 and November 2006 for the 1 Km extent were different. Again, as opposed to the paired Wilcoxon two-sided rank test, this test suggests that time since last flood has some influence on downward fluxes.

Table 6: Flux change in the median downward flux rate between sampling campaigns for each sampling extent.

Extent	Mar-May	May-Nov	Nov-Apr	Mar-Nov	Mar-Apr	May-Apr
10 Km	3.6E-04†	-1.8E-04	-1.1E-04	1.8E-04	6.6E-05	-2.9E-04†
1 Km	3.2E-04†	-4.4E-04†	3.3E-04	-1.2E-04	2.1E-04	-1.1E-04
100 m	-1.1E-04	1.2E-05	7.4E-05	-9.5E-05	-2.1E-05	8.7E-05
40 m	-5.3E-05	-7.8E-06	1.3E-04	-6.1E-05	6.5E-05	1.2E-04

† Median flux rate magnitudes between sampling campaign are statistically different to a 95% significance level based on a non-parametric Wilcoxon rank sum test.

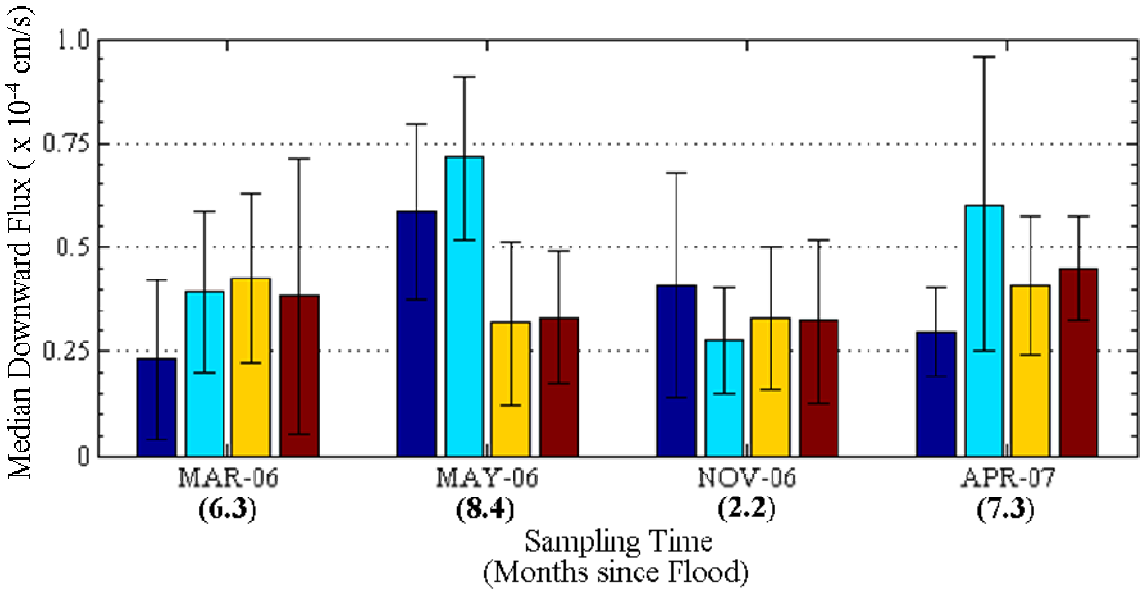

Figure 13: Median flux rate value for sites with downward flux for each sampling extent with respect to sampling campaign. From left to right the 10 Km, 1 Km, 100 m and 40 m extents are first (blue), second (cyan), third (yellow) and forth (brown) bar respectively. Note that color pattern repeats for each sampling campaign. Error bars indicate the 95% confidence intervals based on a bootstrap analysis.

Investigating the median flux rate for sites with upward fluxes (Figure 14) and for sites with downward fluxes (Figure 15) for all extents in a sampling campaign indicates that time since flood has a limited effect on upward fluxes and no significant effect on downward fluxes. Analysis of these groups shows that: 1) there was an increase in upward and downward flux magnitude between March 2006 and May 2006, 2) there was a decrease in upward and downward flux magnitude between May 2006 and November 2006, and 3) there was an increase in downward flux magnitude between November 2006 and April 2007 (Table 7 and 8). This change is also reflected in the ratio of the median downward flux (Figure 15) to the median upward flux (Figure 14) which was 0.45, 0.49, 5.81 and 5.24 for March 2006, May 2006, November 2006 and April 2007, respectively. The ratios suggest that the summer floods changed the relationship of the upward and

downward fluxes during and after the floods of 2006. A Wilcoxon rank sum test (α=0.05) shows that only the median upward flux rate for all sites and extents between May 2006 and November 2006, and May 2006 and April 2007 are different; suggesting that median upward vertical flux exhibited a limited response to the 2006 summer floods. On the other hand the median downward flux results (Figure 15 and Table 8) agree with the paired non-parametric Wilcoxon two-sided signed rank test; suggesting that time since last flood has no significant effect on the overall distribution of downward fluxes.

Table 7: Flux change in the median upward flux rate between sampling campaigns for all sampling extents.

Mar-May	May-Nov	Nov-Apr	Mar-Nov	Mar-Apr	May-Apr
3.4E-04	-8.3E-04†	1.2E-05	-4.8E-04	-4.7E-04	-8.1E-04†

† Median flux rate magnitudes between sampling campaign are statistically different to a 95% significance level based on a non-parametric Wilcoxon rank sum test.

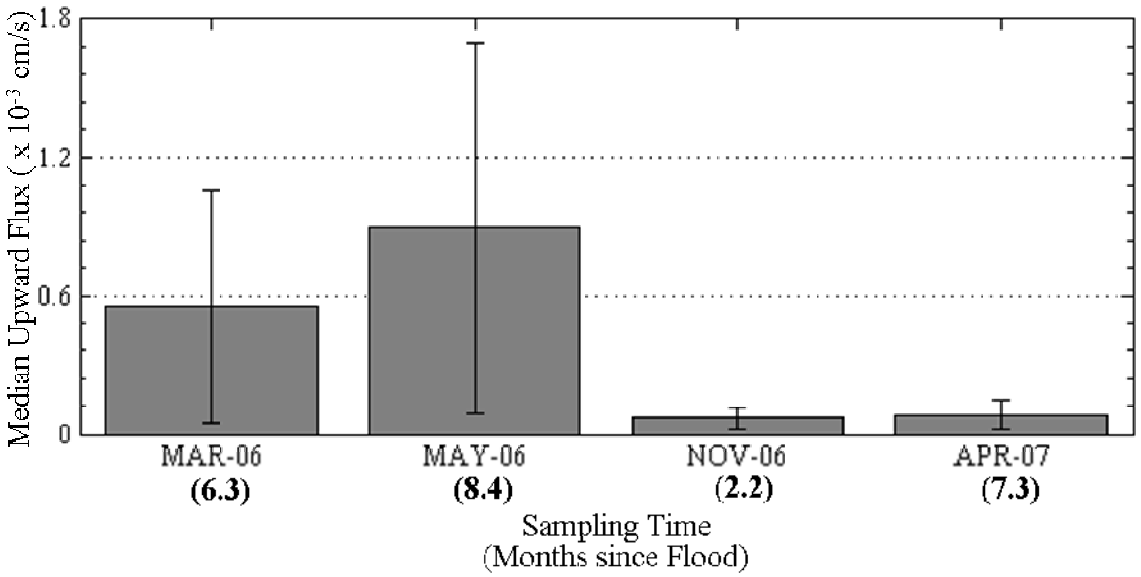

Figure 14: Median flux rate value for sites with upward flux at all extents with respect to sampling campaign. The x axis lists the each sampling campaign. Error bars indicate the 95% confidence intervals based on a bootstrap analysis.

Table 8: Flux change in the median downward flux rate between sampling campaigns for all sampling extents.

Mar-May	May-Nov	Nov Apr	Mar-Nov	Mar-Apr	May-Apr
-4.5E-05	4.4E-05	-4.7E-05	-1.9E-07	-4.7E-05	-2.4E-06

† Median flux rate magnitudes between sampling campaign are statistically different to a 95% significance level based on a non-parametric Wilcoxon rank sum test.

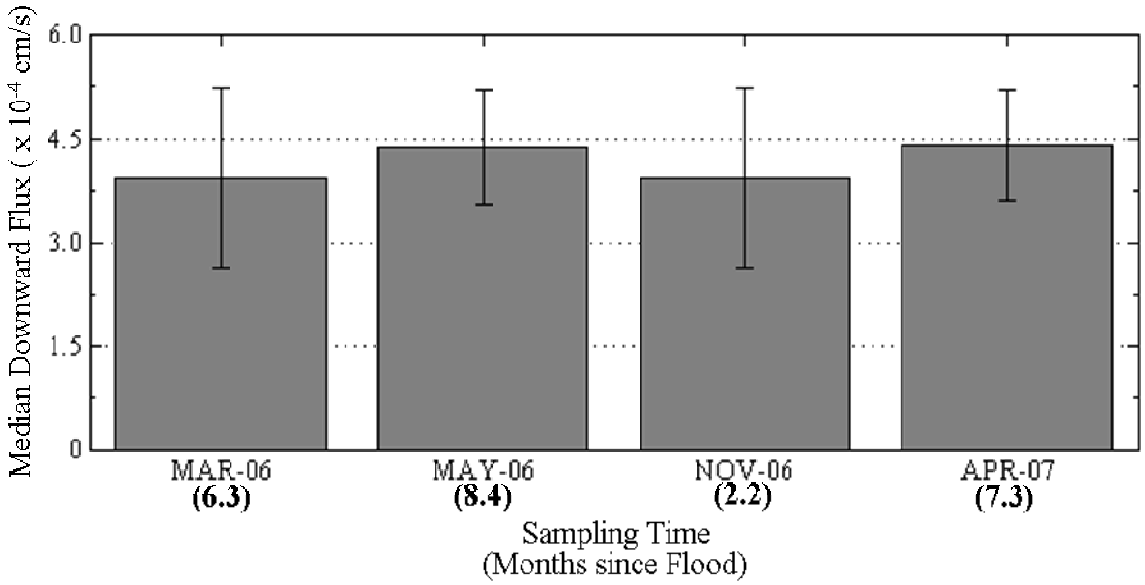

Figure 15: Median flux rate value for sites with downward flux at all extents with respect to sampling campaign. Error bars indicate the 95% confidence intervals based on a bootstrap analysis.

Looking at the median flux rates for all extents in a sampling campaign regardless of flux direction agrees with previous results suggests that time since last flood does not influence vertical fluxes (Figure 16). Although, this group shows that there was: 1) an increase in flux magnitude between March 2006 and May 2006, 2) a decrease in flux magnitude between May 2006 and November 2006, and 3) an increase in flux magnitude between November 2006 and April 2007 (Table 9), none of the differences were significant according to A Wilcoxon rank sum test (α=0.05). Taken as a whole, these

results suggest that even though at individual locations and sampling extents vertical fluxes change in magnitude, direction or both in response to sampling time (time since last flood) the statistical test suggests that overall time since last flood does not significantly influence the observed distribution of vertical fluxes.

Table 9: Flux change in the median flux rate between sampling campaigns for all sampling extents.

Mar-May	May-Nov	Nov Apr	Mar-Nov	Mar-Apr	May-Apr
-4.6E-05	3.9E-05	-1.2E-04	-7.6E-06	-1.3E-04	-8.4E-05

† Median flux rate magnitudes between sampling campaign are statistically different to a 95% significance level based on a non-parametric Wilcoxon rank sum test.

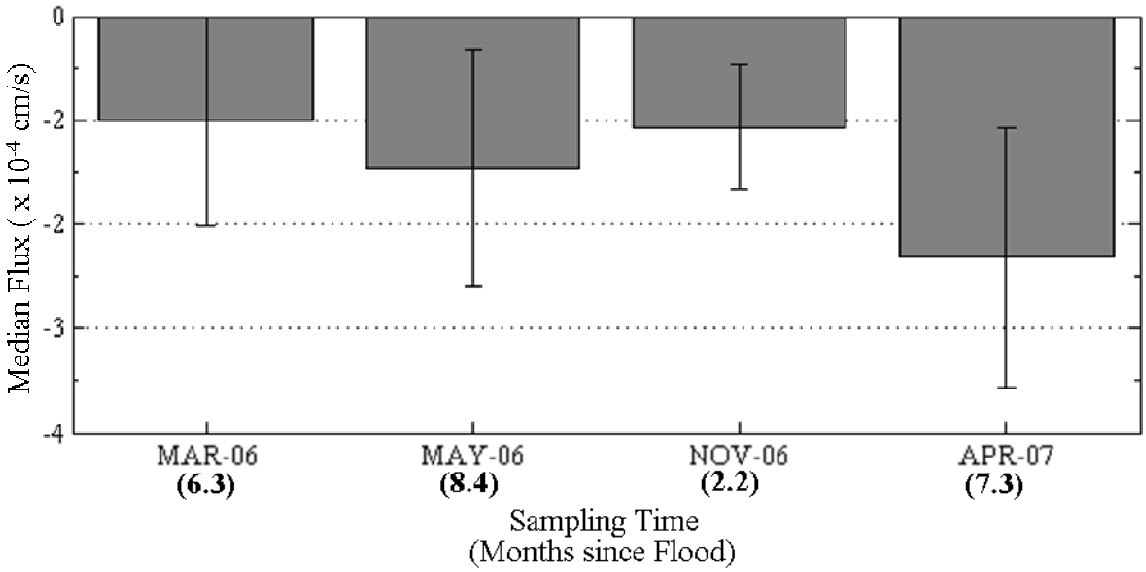

Figure 16: Median flux rate value for all sites and extents. Error bars indicate the 95% confidence intervals based on a bootstrap analysis. Note that negative flux values indicate that the median flux rate is in the downward direction.

3.3 Seepage meter fluxes and Stallman's fluxes

Flux estimates obtained using Stallman's solution vertical fluxes were compared to fluxes measured using seepage meters at select sites of the 1 Km extent during the sampling campaigns of November 2006 and April 2007 (Treese S, personal communication). Seepage meters were deployed around temperature sensor locations. These fluxes were compared to Stallman's estimated fluxes (Figure 17). Seepage meter fluxes were an order of magnitude higher than the fluxes obtained from Stallman's solution (Figure 17). Regardless of direction 62.8% of Stallman's fluxes agree with the direction of flux determined with seepage meters. Also, 82.4% and 50% of Stallman's fluxes agree with the direction of flux determined with seepage meters for the downward and upward flux cases, respectively. These results appear to suggest that Stallman's solution miscalculates upward fluxes more frequently than downward fluxes (Figure 17). One potential source for the difference in these fluxes is the support scale of the measurement. Seepage meter fluxes rely on measuring a change in volume over a set area. The area or support scale for seepage meters is at least an order of magnitude larger than the support scale of temperature measurements. Ignoring instrument or measurement error, this difference tied with the potential high spatial variability of vertical fluxes could cause seepage meters to capture localized high fluxes.

Similar results were observed by Keery et al. (2007). Keery et al. (2007) extended Stallman's solution by utilizing automatic signal processing to process sediment and surface water temperature time series to estimate vertical fluxes at every time step during a 4 month period in the Tern River in Shropshire, England. His flux estimates using

Stallman's solution were on the same order of magnitude as the flux estimates obtained for the San Pedro. Also, Keery et al. (2007) collected flux measurements using seepage meters to support the flux estimates from temperature time series. As opposed to seepage fluxes in the San Pedro River, these fluxes were about an order of magnitude smaller than the fluxes estimated from Stallman's solution. Similar to our results Keery et al. (2007) found that no upward fluxes were observed in locations where analysis of temperature time series predicted upward fluxes.

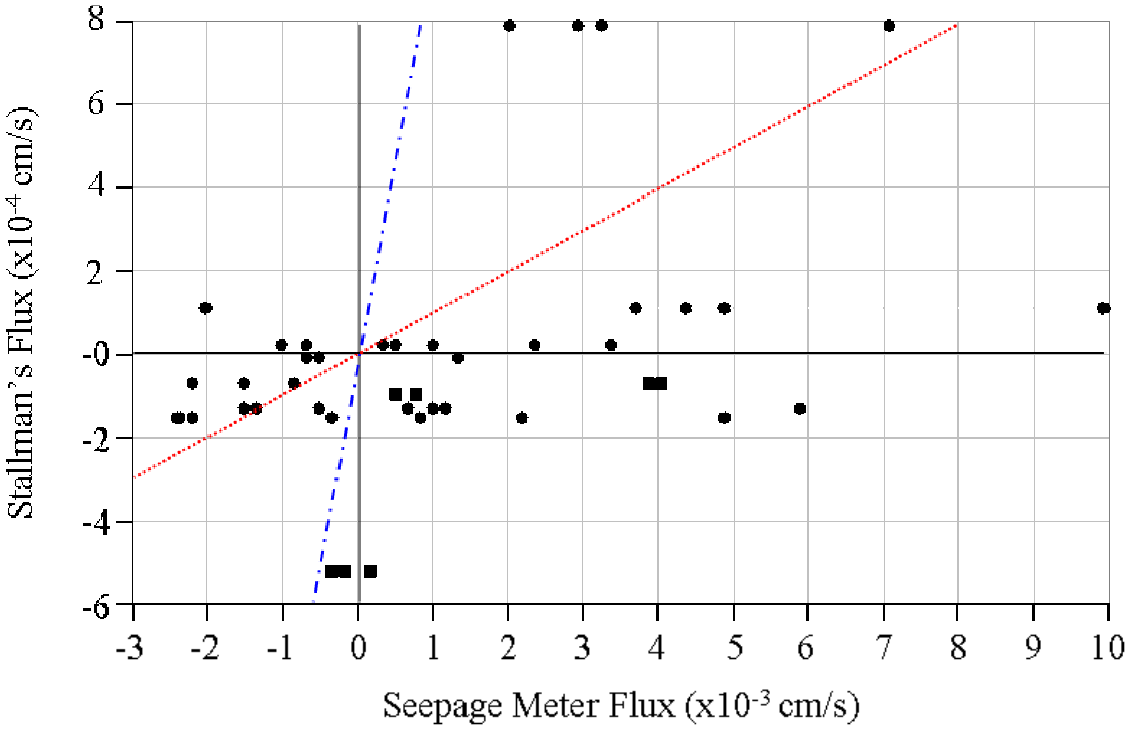

Figure 17: Correlation plot of Stallman's Flux versus measured fluxes using seepage meter. The blue dashed line represents a 1:1 line, while the red solid line represents a 10:1 line. Triangles and squares represent data from November 2006 and April 2006 respectively. Note that negative fluxes indicate downward fluxes. Seepage meter fluxes were obtained from Treese S. (personal communication).

3.4 Geostatistics

At the 10 Km extent, semi-variance rose continually with lag distance only for the sampling campaign of April 2007 (Figure 18-D). At the 1 Km extent, semi-variance was correlated with lag distance for the sampling campaign of March 2006 (Figure 19-A). A random or pure nugget behavior is characterized by a semi-variance that has no structured correlation with lag distance (Figure 18A, 18B, 18C, 19-B, 19-C and 19-D). A continually rising semi-variance with lag distance indicates that vertical flux exhibits spatial dependency. In practical terms this means that vertical flux measurements farther away become constantly more different. The fact that all but one of the 1 Km and 10 Km sampling campaigns semi-variances were spatially independent suggests that no further information other than the point flux estimates was gained from sampling fluxes at those extents and intervals.

For the 100 m extent, semi-variances rose continually with lag distance until it leveled off at a sill (Figure 20B, 20C and 20D) with the exception of March 2006 which exhibited a random behavior (Figure 20A). The lag distance of the sill is called the range and at lag distances greater than the range, vertical fluxes become spatially independent. Thus, the range indicates the distance over which vertical flux values are correlated. The range values (Table 10 and Figure 20) for the 100 m extent for May 2006, November 2006 and April 2007 were 24, 10 and 21 m, respectively. As with the 100 m extent, the 40 m extent semi-variances were correlated with lag distance with the exception of March 2006. But, as opposed to the 100m extent, not all semi-variograms attained a sill

within the maximum lag distance. The range values (Table 10 and Figure 21) for the 40 m extent for November 2006 was 6 m.

At the 100 m and 40 m sampling extent the range values decreases between May 206 and November 2006, and increases between November 2006 and April 2007. The fact that the range appears to be related to time since last flood suggests that the length of continuous upward or downward flux regions increases as time since last flood increases. This result also indicates that as time since last flood increases the spatial heterogeneity of vertical fluxes decreases. This observation is also supported by the decrease in the coefficient of variation between March 2006 and May 2006 as well as between November 2006 and April 2007.

Semi-variograms of the 100 m and 40 m extents (Figure 20 and 21) suggest that the distance of spatial dependence of the vertical flux varies from 6 to 24 m. On the other hand, no spatial dependence was observed in any of the semi-variograms for the 10 Km and 1 Km extents with the exception of April 2007 at the 10 Km extent and March 2006 for the 1 Km extent. These observations, suggests that: 1) the length of continuous upward or downward fluxes is not homogeneous along the study site and, 2) that the identification of either upward or downward fluxes at sampling intervals greater than 6 m is a random process.

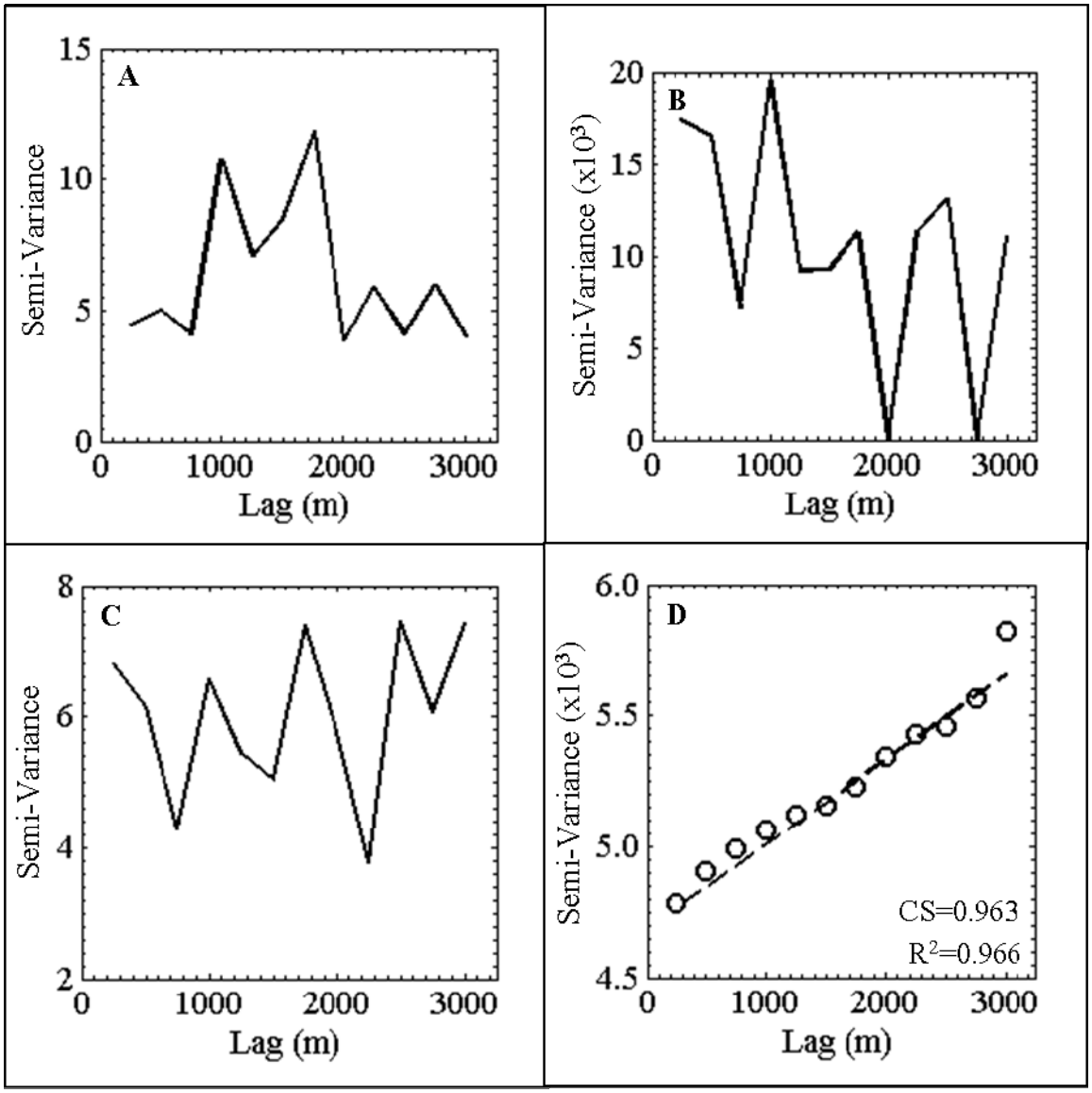

Figure 18: Semi-Variograms of the flux for the 10 Km sampling extent. In the x-axis and y-axis lag distance and semi-variance of the flux, respectively. Dashed line shows the fitted model while solid line shows data to which model could be fitted. Open symbols indicate the data, to which the model was fitted. A) March 2006, random or pure nugget behavior; B) May 2006, random or pure nugget behavior; C) November 2006, random or pure nugget behavior; D) April 2006, linear model. Indices of the linear model are listed on Table 10.

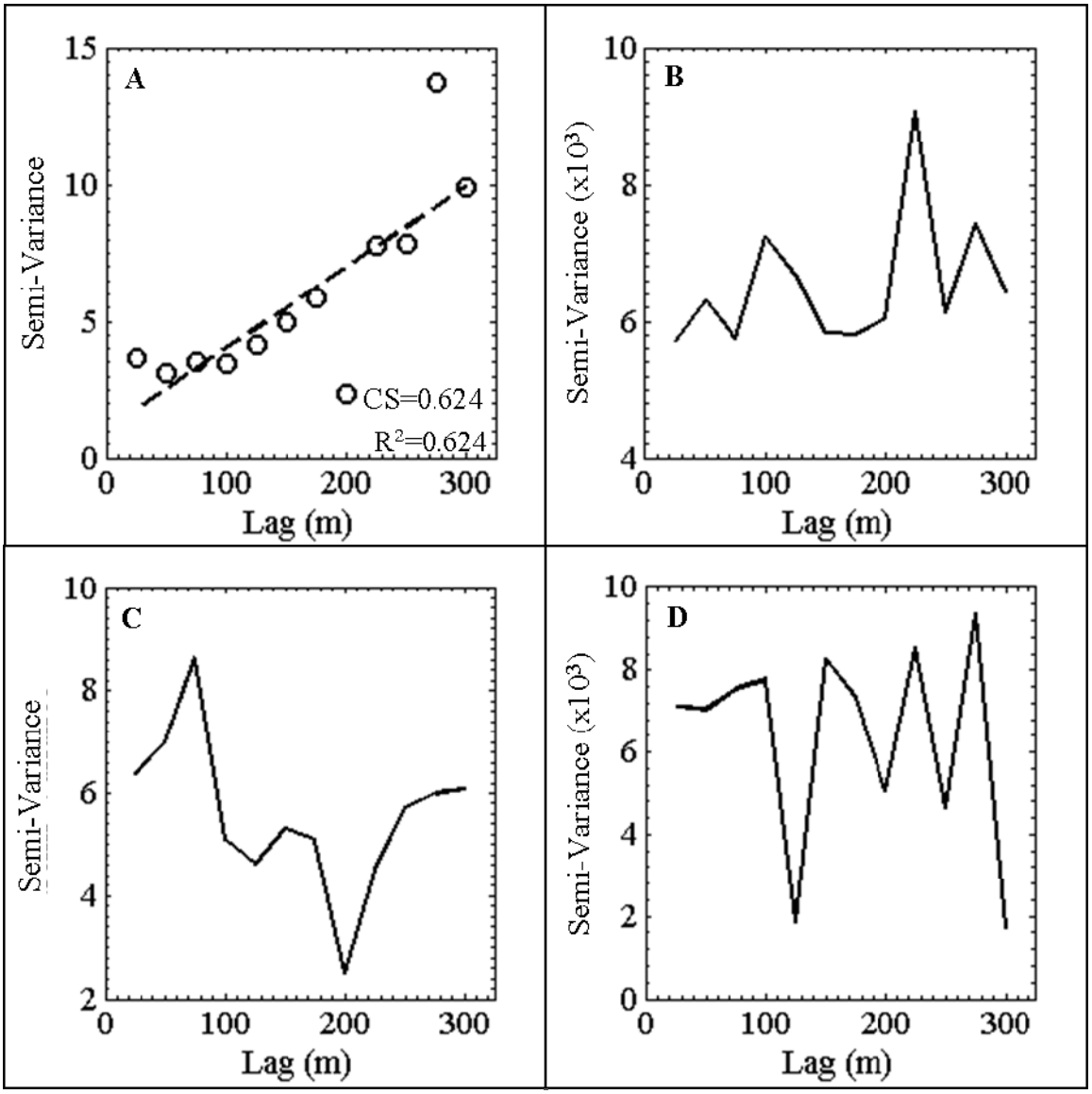

Figure 19: Semi-Variograms of the flux for the 1 Km sampling extent. In the x-axis and y-axis lag distance and semi-variance of the flux, respectively. Solid line shows data to which model could be fitted. Open symbols indicate the data, to which the model was fitted. A)March 2006, linear model; B)May 2006, random or pure nugget behavior; C)November 2006, random or pure nugget behavior; D)April 2006, random or pure nugget behavior. Indices of the linear model is listed on Table 10

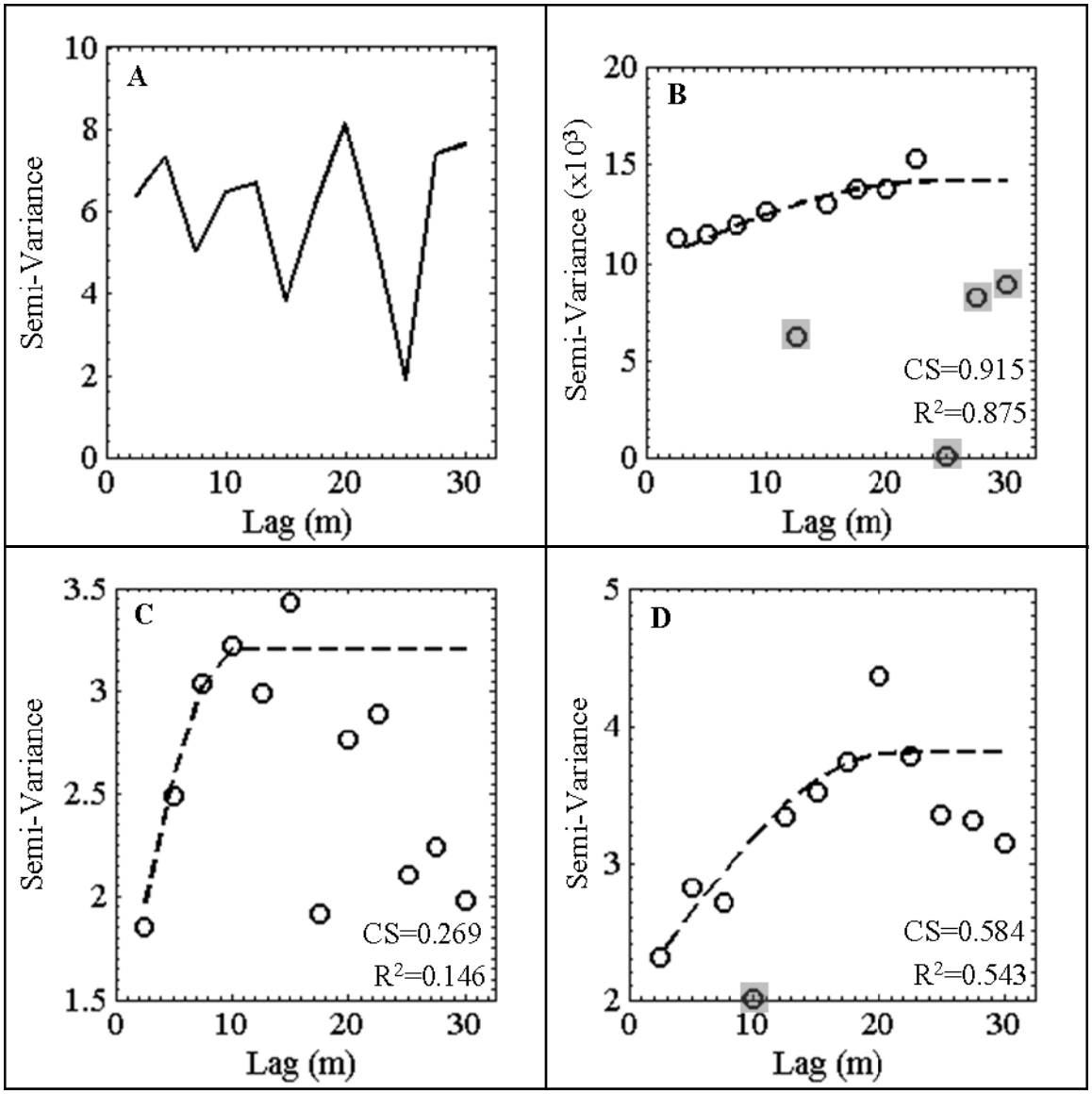

Figure 20: Semi-Variograms of the flux for the 100 m sampling extent. In the x-axis and y-axis lag distance and semi-variance of the flux, respectively. Dashed line shows the fitted model. Open symbols indicate the data, to which the model was fitted. Open symbols covered in a gray square indicate data which was not used in the calculations of R^2 and correlation slope (CS). A)March 2006, random or pure nugget behavior; B)May 2006, spherical model; C)November 2006, spherical model; D)April 2006, spherical model. Indices each model is listed on Table 10

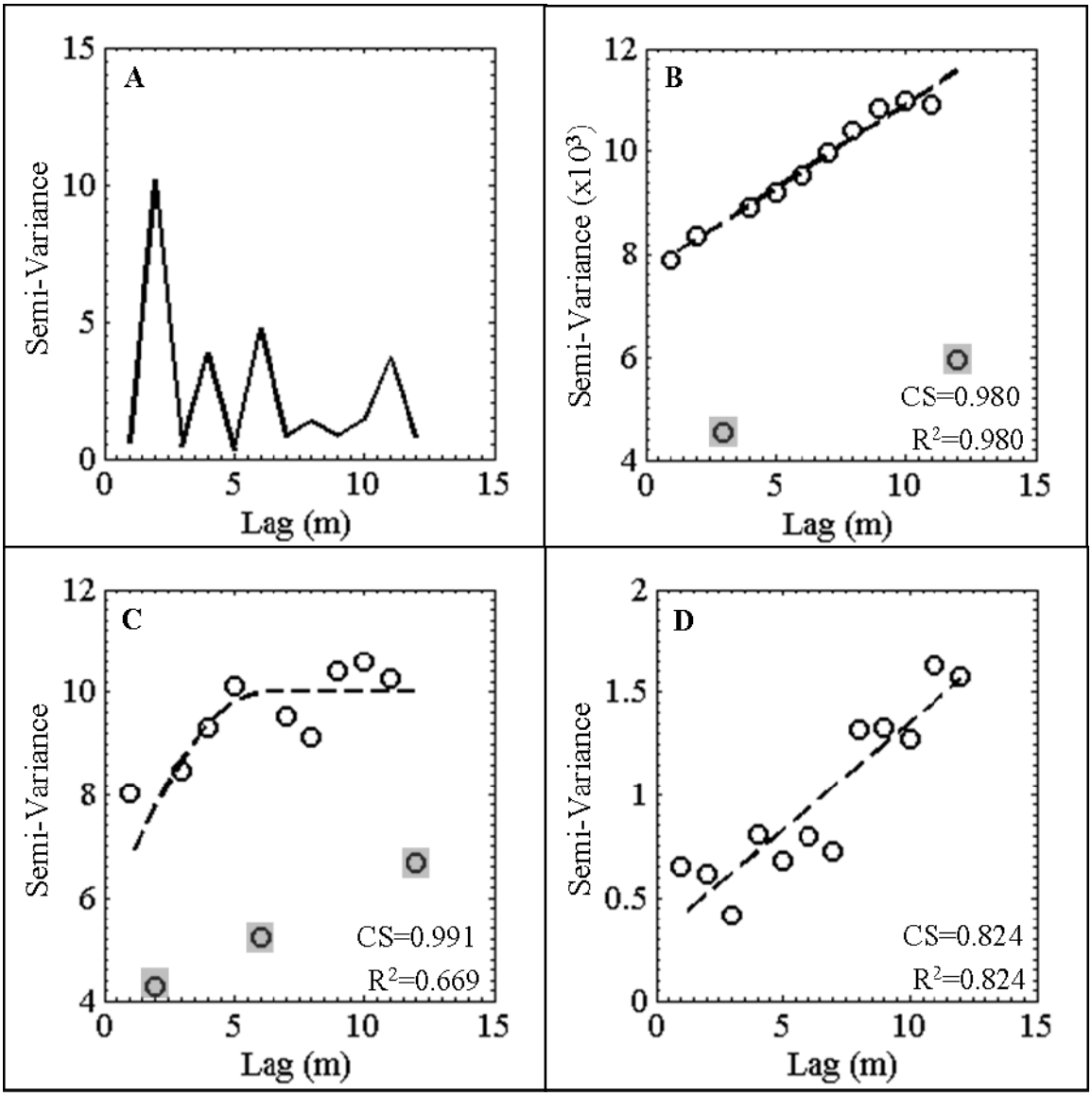

Figure 21: Semi-Variograms of the flux for the 40 m sampling extent. In the x-axis and y-axis lag distance and semi-variance of the flux, respectively. Dashed line shows the fitted model. Open symbols indicate the data, to which the model was fitted. Open symbols indicate the data, to which the model was fitted. Open symbols covered in a gray square indicate data which was not used in the calculations of R2 and correlation slope (CS). A)March 2006, random or pure nugget behavior; B)May 2006, v; C)November 2006, spherical model; D)April 2006, linear model. Indices each model is listed on Table 10

Table 10: Semi-Variogram model indices for all extents and sampling campaigns.

Extent	Date	Months since Flood	Model†	Nugget	Sill	Range (m)	CS‡	R^2
10 Km	Mar-06	6.3	R	…	…	…	…	…
10 Km	May-06	8.4	R	…	…	…	…	…
10 Km	Nov-06	2.2	R	…	…	…	…	…
10 Km	Apr-07	7.3	L	…	…	>3000	0.963	0.966
1 Km	Mar-06	6.3	L	…	…	>300	0.624	0.624
1 Km	May-06	8.4	R	…	…	…	…	…
1 Km	Nov-06	2.2	R	…	…	…	…	…
1 Km	Apr-07	7.3	R	…	…	…	…	…
100 m	Mar-06	6.3	R	…	…	…	…	…
100 m	May-06	8.4	S	10000	14200	24	0.915	0.875
100 m	Nov-06	2.2	S	1.2	3.2	10	0.269	0.146
100 m	Apr-07	7.3	S	2	3.8	21	0.584	0.543
40 m	Mar-06	6.3	R	…	…	…	…	…
40 m	May-06	8.4	L	…	…	>12	0.98	0.98
40 m	Nov-06	2.2	S	5.75	10	6	0.991	0.669
40 m	Apr-07	7.3	L	…	…	>12	0.824	0.824

†Model refers to the model semi-variogram type fitted: R = Random, L = Linear, S = Spherical.

‡Correlation slope (CS) refers to the slope of a linear regression between observed semi-variances and fitted semi-variances. Ellipses indicate that a spherical semi-variogram model could not be fitted.

4 DISCUSSION

4.1 Vertical exchange, time since flood and stream discharge

A daily stream hydrograph of the San Pedro River at Charleston (Figure 5) reveals that this hydrologic system has a period of somewhat steady streamflow that begins mid-October and ends late March to early April. After this "steady" period, a marked decline in streamflow is observed that begins late March to early April and ends mid-June. The marked decline in streamflow can be attributed to the combined effects of increased transpiration from the riparian vegetation and increased potential evaporation due to the increase of ambient temperatures. In the San Pedro River during the study period, streamflow was inversely related to time since last flood (Figure 22).

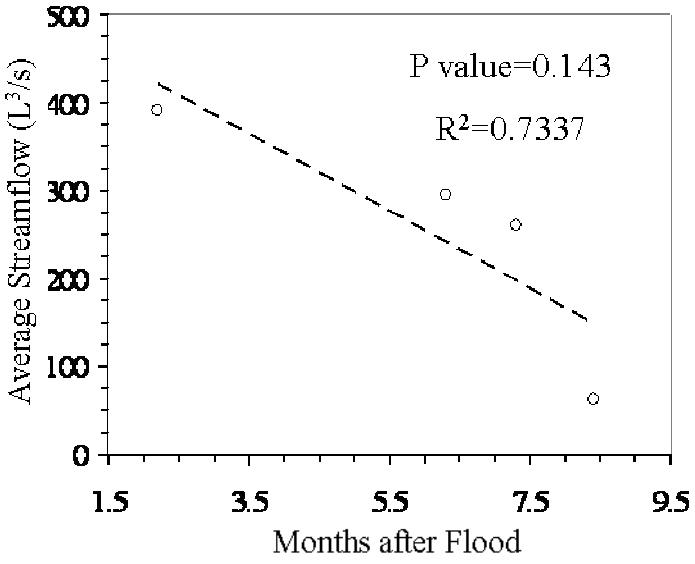

Figure 22: Correlation plot of average streamflow versus the months after flood for each sampling campaign. Average streamflow was calculated by averaging the average daily streamflow values from USGS gauging station San Pedro River at Charleston for the two-weeks covering the temperature sensor deployment.

Certainly a decrease in streamflow will be accompanied by a decrease in river stage which would alter near stream hydraulic gradients. A change in the hydrologic gradient will trigger changes in the magnitude and direction of vertical fluxes. Because of this, a decrease in the magnitude of the downward vertical fluxes and an increase in the magnitude of upward fluxes were expected as time since last flood increased and streamflow decreased. The data shows that at point scales fluxes do change in magnitude and/or direction between sampling campaigns and sampling locations. But, analysis of the distribution of fluxes shows that neither streamflow nor time since last flood influence vertical fluxes. Correlation plots between vertical flux, average streamflow and time since last flood suggest that the median magnitudes of downward and upward flux increase as time since last flood increases and streamflow decreases. However, these correlations are not statistically significant. These results further support the finding that time since last flood and streamflow do not significantly affect the overall distribution of vertical fluxes during the study period.

4.2 Spatial structure of streambed fluxes

Vertical fluxes are highly variable in space and time. At point scales, fluxes change in magnitude and/or direction between sampling campaigns and sampling locations. The vertical fluxes have a coefficient of variation for each sampling campaign of 177.10, 8.09, 124.89 and 15.15 for March 2006, May 2006, November 2006, and April 2007, respectively. The relative decrease, increase and decrease of the coefficient of variation between March 2006 and May 2006, May 2006 and November 2006, and November 2006 and April 2007, respectively suggests that the spatial distribution of vertical fluxes

becomes more homogeneous as time since last flood increases and streamflow decreases. At the same time, semi-variograms show that vertical flux estimates at sampling extents of 10 Km and 1 Km are spatially independent (Figures 18 and 19) while vertical fluxes for the sampling extents of 100 m and 40m exhibited spatial dependence (Figures 20 and 21). In addition, at 100 m and 40 m sampling extent the semi-variogram range values decreased between May 2006 and November 2006, and increased between November 2006 and April 2007. The fact that the range values are related to time since last flood suggests that the length of continuous upward or downward flux regions increases as time since last flood increases. This finding further supports the idea that the spatial distribution of vertical fluxes becomes more homogeneous as time since last flood increases.

Researchers have used the influence of stream geomorphic structure to qualitatively describe stream aquifer interactions. *Harvey and Bencala* [1993] identified the change in streambed slope and the change of streambed concavity as an important control on vertical flux direction. Riffles are usually steeper in slope than runs. Therefore at run-riffle interfaces (concave down) there is usually a downward flux while at the riffle-run or riffle-pool interfaces (concave up) there is usually an upward flux. *Dent et al.* [2001] used this geomorphic characteristic to infer direction of vertical exchange and its effect on stream water chemistry. During the current study, contrary to expectations no clear association between run-riffle interfaces and vertical fluxes was observed. The data does show that runs are associated with higher magnitude downward fluxes than riffles.

4.3 Implications

Water exchange between surface and ground waters is an important control on stream water composition [*Dent et al.,* 2001; *Jones et al.,* 1995c; *Valett et al.,* 1994]. Whether the location of these exchanges will act as sources or sinks of nutrients will depend on the directionality of exchange [*Dent et al.,* 2001; *Jones et al.,* 1995c; *Valett et al.,* 1994]. Therefore, observations of exchange direction are important in order to have a basic understanding of nutrient and chemical processes in the stream. In previous, studies the determination of the direction of exchange was based on measurements of hydraulic gradients (energy potential) or by linking the geomorphic structure of the stream with direction of exchange. These observations, although useful, are unable to describe mass exchange in stream-aquifer interactions. Understanding location, extent and magnitude of vertical fluxes will enable better characterization of water and solute mass balance in the stream.

The application of Stallman's analytical solution in the San Pedro River to estimate vertical fluxes suggests the overall distribution of vertical fluxes is unaffected by time since last flood and streamflow. On the other hand, the spatial structure of vertical fluxes appears to be influenced by time since last flood and streamflow. The data suggest that the spatial distribution of vertical fluxes becomes more homogeneous as time since last flood increases. Semi-variograms showed that the length of continuous upward or downward flux was not homogeneous along the study site and the identification of spatially structured vertical fluxes is highly dependent on sampling intervals and the extent of sampling. This increase in the spatial structure of vertical fluxes and reduced

streamflow might explain increases of nutrient concentration in streamwater as time since last flood increases, observed in other semi arid streams [*Dent and Grimm,* 1999; *Dent et al.,* 2001; *Holmes et al.,* 1994; *Jones et al.,* 1995a]. In addition, the increase in vertical flux homogeneity as time since last flood increases might alter nutrient spiraling (the cycling of nutrients while being carried downstream) by increasing nutrient uptake lengths in the stream.

Any temperature based method of estimating flux direction and magnitude at the streambed interface [*Becker et al.,* 2004; *Hatch et al.,* 2006; *Keery et al.,* 2007; *Silliman and Booth,* 1993; *Silliman et al.,* 1995; *Stallman,* 1965] is a vertical line average estimate of that flux between temperature measuring points. In the San Pedro River, distances of spatial dependence ranged from 6m to 24m and varied with sampling scale and time. Any estimate of flux done at a larger distance would limit the information gained to only that of the point estimate itself. *Becker et al.* [2004] found that the point estimates of ground water flux in Ischua Creek in New York were 1 to 2 orders of magnitude smaller than area measurements of ground water flux. He concluded that the difference was caused by localized high flux groundwater inputs into the stream. *Conant* [2004] mapped the distributions of fluxes of a sandy stream by combining measurements of temperature at the streambed and hydraulic testing using mini-piezometers. Using this method *Conant* [2004] found that localized high flux regions covered 3.8% of the streambed area but contributed to approximately 20-24% of the total discharge of the stream reach. In the San Pedro River, area measurements of upward vertical flux (seepage meters) were an order of magnitude higher than point estimates of fluxes. Although, localized high

vertical fluxes could explain the differences seen in the San Pedro River, Stallman's solution poorly estimates high magnitude upward fluxes.

Certainly, the type of vertical flux mapping done by *Conant* [2004] would have to be one of the most desirable pieces of information to perform water and solute mass balance in a stream. Still, deploying this methodology on reaches greater than a few hundred meters long is difficult and time consuming. At these scales, remotely sensed infrared imagery used in conjunction with high resolution distributed temperature sensing (DTS) coupled with energy budget modeling would be more useful [*Loheide and Gorelick,* 2006; *Selker et al.,* 2006].

5 CONCLUSION

This research utilizes temperature oscillation as a tracer of vertical water fluxes by applying Stallman's analytical solution to a series of temperature time series recorded at the stream and 10 cm beneath the streambed surface on the San Pedro River. A parameter perturbation analysis showed that, Stallman's analytical solution has the potential of estimating both directionality and magnitude of vertical fluxes at point scale. But, Stallman's analytical solution fails to give correct estimates of upward fluxes as the magnitude of these upward fluxes increase. Comparing Stallman's fluxes with fluxes measured using seepage meters showed that: 1) Stallman's fluxes were an order of magnitude lower than the fluxes measured using seepage meters and 2) the disagreement is more pronounced for upward fluxes. However, when using Stallman's analytical solution to infer flux from temperature time series, it is important to: 1) understand that strong upward fluxes will prevent diurnal heat pulses to propagate downward and 2) ensure that measurements of temperature oscillations at depth are taken with adequate resolution to quantify the amplitude fluctuations and timing of the heat pulse peak.

Results of applying Stallman's analytical solution in the San Pedro River have shown that vertical fluxes vary in space and time. In the San Pedro River during the period of study, streamflow decreases as time since last flood increased. During this time the distribution of vertical fluxes did not change significantly. Variations in both flux directionality and magnitude were observed at distances of 1 m and time lengths of 2.1 months. The geomorphology of the stream also affected the magnitude of vertical fluxes. At the 100m and 40 m extents, runs had higher downward fluxes than riffles. Semi-

variograms showed that vertical fluxes exhibited spatial dependence at the 100 m and 40 m extents. The spatial dependence ranged from 6 to 24 m when flux estimates were done at intervals of 1 to 2.5 m. Overall, flux estimates at intervals of 25 m and greater exhibited a random behavior with no spatial structure.

Research has shown that the water exchange between surface and ground waters is an important control on stream water chemistry [*Dent et al.,* 2001; *Jones et al.,* 1995c; *Valett et al.,* 1994]. At the same time, it is evident that understanding location, extent and magnitude of vertical fluxes enables a characterization of water and solute mass balance in the stream. In the San Pedro River, semi-variogram range values appear to be related to time since last flood. This relationship suggests that the length of continuous upward or downward flux regions increases as time since last flood increases. This result also indicates that as time since last flood increases the spatial heterogeneity of vertical fluxes decreases. This change has the potential of altering nutrient spiraling uptake lengths and might explain increases of nutrient concentration in streamwater as observed in other semi arid streams [*Dent and Grimm,* 1999; *Dent et al.,* 2001; *Holmes et al.,* 1994; *Jones et al.,* 1995a]

APENDIX: MATLAB CODE TO APPLY STALLMAN'S ANALYTAL SOLUTION

```
function [R10K,R1K,R100M,R40M,q10K, q1K, q100M, q40M]=calcq_stch(MAY);
%MAY=The input matrix for any sampling period
%The output files that start with R are the results files for each scale
%The output files that start with q are the structured files containing the
%distribution of flux values.
%% Set Important Parameters
k=2.375/(4.18*100);%heat conductivity of Saturated sand (cal cm-1 s-1 C-1)
k_uns=0.2500/(4.18*100);%heat conductivity standard deviation
thetha=1;  % since porosity is not used then =1
z=10; %Depth of Sensor in cm
z_uns=5;%Depth uncertainty
minlag=1800;%Absolute value of minimum Acceptable lag for calculation in seconds
minamp=0.375; %Minimum acceptable sediment temperature amplitude.
tau=24*60*60; %period of oscillation in seconds
iter=150; %Number of iterations.
%% Start Analysis
for S=[10000 1000 100 40]  % To Loop on all Scales
   [RI,CI]=find(MAY(:,6)==S);
   MAYTEMP=MAY(RI(:),:); %To process only the selected scale
   MAY_SITE=unique(MAYTEMP(:,7)); %To create a list of unique site numbers
   L=length(MAY_SITE);
   for it=1:iter %To loop with the total number of iterations
      clear Results fit_W_Ampl fit_W_phase fit_W_mean E_W...
         fit_S_Ampl fit_S_phase fit_S_mean E_S indx zr zc
      for i=1:L; %To loop on all sites
         [RI,CI]=find(MAYTEMP(:,7)==MAY_SITE(i));
         MAYTEMP_SITE=MAYTEMP(RI(:),:);
         [RI,CI]=find(MAYTEMP_SITE(:,4)==6 & MAYTEMP_SITE(:,5)==0);
         MAYTEMP_SITE=MAYTEMP_SITE(RI:length(MAYTEMP_SITE),:);
         LT=floor(length((MAYTEMP_SITE-RI(1,1)))/96);
         for j=0:LT-1;
            T=(MAYTEMP_SITE(96*j+1:96*j+97,:));%Use only this line to use
temperature data as is....
            %Uncoment the one below to apply normal distribution of uncertainty
            T(:,8)=normrnd(T(:,8),1/(2*2.57583)); %So that 99%percent of the data fall
withing 2.57583 standard deviation
            T(:,9)=normrnd(T(:,9),1/(2*2.57583));
            %% Fit the surface water data to Sin Wave and extract coefficients
            f = fittype('v+a*sin(2*pi*(x-b)/96)');
            fit_W = fit([1:97]',T(:,9),f,'StartPoint',[(max(T(:,9))-...
               min(T(:,9)))/2 48 mean(T(:,9))],'Lower', [0 0 0] );
```

```
            fit_W_coeff=coeffvalues(fit_W);
            fit_W_int=confint(fit_W);
            if fit_W_int(1,1)<0;
               fit_W_int(1,1)=0;
            end;
            fit_W_int_Ampl(i,j+1)=(fit_W_int(2,1)-fit_W_int(1,1))/2;
            fit_W_int_phase(i,j+1)=(fit_W_int(2,2)-fit_W_int(1,2))/2;
            fit_W_Ampl(i,j+1)=fit_W_coeff(1,1);
            fit_W_phase(i,j+1)=fit_W_coeff(1,2);
            fit_W_mean(i,j+1)=fit_W_coeff(1,3);
            %% Fit the surface water data to Sin Wave and extract coefficients
            fit_S = fit([1:97]',T(:,8),f,'StartPoint',[(max(T(:,8))-min(T(:,8)))/2 48
mean(T(:,9))],'Lower', [0 0 0] );
            fit_S_coeff=coeffvalues(fit_S);
            fit_S_int=confint(fit_S);
            if fit_S_int(1,1)<0;
               fit_S_int(1,1)=0;
            end;
            fit_S_int_Ampl(i,j+1)=(fit_S_int(2,1)-fit_S_int(1,1))/2;
            fit_S_int_phase(i,j+1)=(fit_S_int(2,2)-fit_S_int(1,2))/2;
            fit_S_Ampl(i,j+1)=fit_S_coeff(1,1);
            fit_S_phase(i,j+1)=fit_S_coeff(1,2);
            fit_S_mean(i,j+1)=fit_S_coeff(1,3);
            %F_S=feval(fit_S,[1:97]');
            %E_S(i,j+1)=(sum((F_S-T(:,8)).^2)/length(F_S)).^2;
            %T_All=[T(:,8:9) F_S F_W];
            %plot(T_All(1:97,1:4), 'DisplayName', 'T_All(1:97,1:4)',
'YDataSource','T_All(1:97,1:4)'); figure(gcf)
         end;
         Results(i,:)=T(1,1:7); %This aray stores Month, Day, Year,Hour,Minute, Scale
and Site at the beggining of the observation period on columns 1 thru 7
      end;
      if S==10000
         R10K=Results;
         R10K(:,8:9)=0;
         DTW_F=fit_W_Ampl;
         DTS_F=fit_S_Ampl;
         DTW_F=normrnd(DTW_F,fit_S_int_Ampl/(2*1.95996)); %Uncertain DTW
         DTS_F=normrnd(DTS_F,fit_S_int_Ampl/(2*1.95996)); %Uncertain DTS
         indx=find(DTS_F(:)<0);
         DTS_F(indx)=0;
         indx=find(DTW_F(:)<0);
         DTW_F(indx)=0;
         clear indx;
```

```
Tw=normrnd(fit_W_phase,(fit_W_int_phase/(2*1.95996))); %Uncertain Tw
Ts=normrnd(fit_S_phase,(fit_S_int_phase/(2*1.95996))); %Uncertain Ts
LAGt_F=(Ts-Tw)*(15*60);%This correspond to Time Lag in seconds temporary
indx=find(LAGt_F(:)<-1*minlag);
[zr,zc]=find(LAGt_F<0);
LAGt_F(indx)=86400+LAGt_F(indx);
clear indx
indx=find(LAGt_F(:)<minlag);
LAGt_F(indx)=0;
[zr,zc]=find(LAGt_F==0);
zu=normrnd(z,z_uns/(2*1.95996)); %Uncertain z
ku=normrnd(k,k_uns); %uncertain k
a_F=(log10(DTS_F./DTW_F))/-zu;
b_F=(2*pi*LAGt_F)/(tau*zu);
v_F=ku*((b_F.^2)-(a_F.^2))./a_F;
indx=find(DTS_F(:)<=minamp);
v_F(indx)=-1.7E-3;
q_F(:,:,it)=v_F*-thetha;
[ri,ci,zi]=size(q_F);
if it==iter;
   for f=1:ri;
      for ff=1:zi;
         q_Ft=q_F(f,:,ff);
         q_Ft=sort(q_Ft,2);
         q_Fnan=isnan(q_Ft);
         c_Fnan=sum(q_Fnan,2);
         if ff==1;
            q=q_Ft(:,1:ci-c_Fnan);
            qq.([char(81) int2str(f)])=q;
         else
            q=[q q_Ft(:,1:ci-c_Fnan)];
            q=sort(q);
            qq.([char(81) int2str(f)])=q;
            if ff==zi;
               q_F_median(f,1)=median(q);
               q_F_average(f,1)=mean(q);
               q_F_var(f,1)=var(q);
               q_F_n(f,1)=length(q);
               q_F_std(f,1)=std(q);              %Standard Deviation
               low(f,1)=ceil(0.025*(q_F_n(f,1)+1));   %low rank
               hi(f,1)=floor(0.975*(q_F_n(f,1)+1));   %hi rank
               zscore(f,1)=(q(hi(f,1))-q(low(f,1)))/2;%Distribution z score
               SE(f,1)=q_F_std(f,1)/sqrt(q_F_std(f,1));%Standard Error
               ConfInt(f,1)=zscore(f,1)*SE(f,1);
```

```
                    end;
                end;
            end;
        end;
        q10K=qq;
        R10K(:,12)=(sqrt(q_F_var)./sqrt(q_F_n-1)).*tinv(0.95,(q_F_n-
1));%95%Confidence Bounds T-dist
        R10K(:,11)=ConfInt;                         %95%Confidence Interval
unassumed dist
        R10K(:,9)=q_F_average;
        R10K(:,10)=q_F_median;
        R10K(:,13)=q_F_std;
        R10K(:,14)=q_F_n;
        %R10K=[R10K q_F];
        clear DTW_F DTS_F Tw Ts LAGt_F a_F b_F v_F q_F_median q_F_average
...
            q_F_var q_F_n q_F q_F_std q_F low hi zscore SE ConfInt indx zr zcm zu ku
ri ci zi fit_S_int_Ampl...
            fit_W_int_Ampl fit_W_Ampl fit_S_Ampl fit_S_int_phase...
            fit_W_int_phase qq q
        disp('Done with scale:')
        disp(S)
        toc
    end;
elseif S==1000
    R1K=Results;
    R1K(:,8:9)=0;
    DTW_F=fit_W_Ampl;
    DTS_F=fit_S_Ampl;
    DTW_F=normrnd(DTW_F,fit_S_int_Ampl/(2*1.95996)); %Uncertain DTW
    DTS_F=normrnd(DTS_F,fit_S_int_Ampl/(2*1.95996)); %Uncertain DTS
    indx=find(DTS_F(:)<0);
    DTS_F(indx)=0;
    indx=find(DTW_F(:)<0);
    DTW_F(indx)=0;
    clear indx;
    Tw=normrnd(fit_W_phase,(fit_W_int_phase/(2*1.95996))); %Uncertain Tw
    Ts=normrnd(fit_S_phase,(fit_S_int_phase/(2*1.95996))); %Uncertain Ts
    LAGt_F=(Ts-Tw)*(15*60);%This correspond to Time Lag in seconds temporary
    indx=find(LAGt_F(:)<-1*minlag);
    [zr,zc]=find(LAGt_F<0);
    LAGt_F(indx)=86400+LAGt_F(indx);
    clear indx
    indx=find(LAGt_F(:)<minlag);
```

```
LAGt_F(indx)=0;
[zr,zc]=find(LAGt_F==0);
zu=normrnd(z,z_uns/(2*1.95996)); %Uncertain z
ku=normrnd(k,k_uns); %uncertain k
a_F=(log10(DTS_F./DTW_F))/-zu;
b_F=(2*pi*LAGt_F)/(tau*zu);
v_F=ku*((b_F.^2)-(a_F.^2))./a_F;
indx=find(DTS_F(:)<=minamp);
v_F(indx)=-1.7E-3;
q_F(:,:,it)=v_F*-thetha;
[ri,ci,zi]=size(q_F);
if it==iter;
   for f=1:ri;
      for ff=1:zi;
         q_Ft=q_F(f,:,ff);
         q_Ft=sort(q_Ft,2);
         q_Fnan=isnan(q_Ft);
         c_Fnan=sum(q_Fnan,2);
         if ff==1;
            q=q_Ft(:,1:ci-c_Fnan);
            qq.([char(81) int2str(f)])=q;
         else
            q=[q q_Ft(:,1:ci-c_Fnan)];
            q=sort(q);
            qq.([char(81) int2str(f)])=q;
            if ff==zi;
               q_F_median(f,1)=median(q);
               q_F_average(f,1)=mean(q);
               q_F_var(f,1)=var(q);
               q_F_n(f,1)=length(q);
               q_F_std(f,1)=std(q);              %Standard Deviation
               low(f,1)=ceil(0.025*(q_F_n(f,1)+1));    %low rank
               hi(f,1)=floor(0.975*(q_F_n(f,1)+1));    %hi rank
               zscore(f,1)=(q(hi(f,1))-q(low(f,1)))/2; %Distribution z score
               SE(f,1)=q_F_std(f,1)/sqrt(q_F_std(f,1));%Standard Error
               ConfInt(f,1)=zscore(f,1)*SE(f,1);
            end;
         end;
      end;
   end;
   q1K=qq;
   R1K(:,12)=(sqrt(q_F_var)./sqrt(q_F_n-1)).*tinv(0.95,(q_F_n-
1));%95%Confidence Bounds T-dist
```

```
            R1K(:,11)=ConfInt;                          %95%Confidence Interval
unassumed dist
            R1K(:,9)=q_F_average;
            R1K(:,10)=q_F_median;
            R1K(:,13)=q_F_std;
            R1K(:,14)=q_F_n;
            %R1K=[R1K q_F];
            clear DTW_F DTS_F Tw Ts LAGt_F a_F b_F v_F q_F_median q_F_average
...
              q_F_var q_F_n q_F q_F_std q_F low hi zscore SE ConfInt indx zr zcm zu ku
ri ci zi fit_S_int_Ampl...
              fit_W_int_Ampl fit_W_Ampl fit_S_Ampl fit_S_int_phase...
              fit_W_int_phase qq q
            disp('Done with scale:')
            disp(S)
            toc
          end;
        elseif S==100
          R100M=Results;
          R100M(:,8:9)=0;
          DTW_F=fit_W_Ampl;
          DTS_F=fit_S_Ampl;
          DTW_F=normrnd(DTW_F,fit_S_int_Ampl/(2*1.95996)); %Uncertain DTW
          DTS_F=normrnd(DTS_F,fit_S_int_Ampl/(2*1.95996)); %Uncertain DTS
          indx=find(DTS_F(:)<0);
          DTS_F(indx)=0;
          indx=find(DTW_F(:)<0);
          DTW_F(indx)=0;
          clear indx;
          Tw=normrnd(fit_W_phase,(fit_W_int_phase/(2*1.95996))); %Uncertain Tw
          Ts=normrnd(fit_S_phase,(fit_S_int_phase/(2*1.95996))); %Uncertain Ts
          LAGt_F=(Ts-Tw)*(15*60);%This correspond to Time Lag in seconds temporary
          indx=find(LAGt_F(:)<-1*minlag);
          [zr,zc]=find(LAGt_F<0);
          LAGt_F(indx)=86400+LAGt_F(indx);
          clear indx
          indx=find(LAGt_F(:)<minlag);
          LAGt_F(indx)=0;
          [zr,zc]=find(LAGt_F==0);
          zu=normrnd(z,z_uns/(2*1.95996)); %Uncertain z
          ku=normrnd(k,k_uns); %uncertain k
          a_F=(log10(DTS_F./DTW_F))/-zu;
          b_F=(2*pi*LAGt_F)/(tau*zu);
          v_F=ku*((b_F.^2)-(a_F.^2))./a_F;
```

```
indx=find(DTS_F(:)<=minamp);
v_F(indx)=-1.7E-3;
q_F(:,:,it)=v_F*-thetha;
[ri,ci,zi]=size(q_F);
if it==iter;
   for f=1:ri;
      for ff=1:zi;
         q_Ft=q_F(f,:,ff);
         q_Ft=sort(q_Ft,2);
         q_Fnan=isnan(q_Ft);
         c_Fnan=sum(q_Fnan,2);
         if ff==1;
            q=q_Ft(:,1:ci-c_Fnan);
            qq.([char(81) int2str(f)])=q;
         else
            q=[q q_Ft(:,1:ci-c_Fnan)];
            q=sort(q);
            qq.([char(81) int2str(f)])=q;
            if ff==zi;
               q_F_median(f,1)=median(q);
               q_F_average(f,1)=mean(q);
               q_F_var(f,1)=var(q);
               q_F_n(f,1)=length(q);
               q_F_std(f,1)=std(q);              %Standard Deviation
               low(f,1)=ceil(0.025*(q_F_n(f,1)+1));    %low rank
               hi(f,1)=floor(0.975*(q_F_n(f,1)+1));    %hi rank
               zscore(f,1)=(q(hi(f,1))-q(low(f,1)))/2; %Distribution z score
               SE(f,1)=q_F_std(f,1)/sqrt(q_F_std(f,1));%Standard Error
               ConfInt(f,1)=zscore(f,1)*SE(f,1);
            end;
         end;
      end;
   end;
   q100M=qq;
   R100M(:,12)=(sqrt(q_F_var)./sqrt(q_F_n-1)).*tinv(0.95,(q_F_n-
1));%95%Confidence Bounds T-dist
   R100M(:,11)=ConfInt;                          %95%Confidence Interval
unassumed dist
   R100M(:,9)=q_F_average;
   R100M(:,10)=q_F_median;
   R100M(:,13)=q_F_std;
   R100M(:,14)=q_F_n;
   %R100M=[R100M q_F];
```

```
            clear DTW_F DTS_F Tw Ts LAGt_F a_F b_F v_F q_F_median q_F_average
...
                q_F_var q_F_n q_F q_F_std q_F low hi zscore SE ConfInt indx zr zcm zu ku
ri ci zi fit_S_int_Ampl...
                fit_W_int_Ampl fit_W_Ampl fit_S_Ampl fit_S_int_phase...
                fit_W_int_phase qq q
            disp('Done with scale:')
            disp(S)
            toc
        end;
    elseif S==40
        R40M=Results;
        R40M(:,8:9)=0;
        DTW_F=fit_W_Ampl;
        DTS_F=fit_S_Ampl;
        DTW_F=normrnd(DTW_F,fit_S_int_Ampl/(2*1.95996)); %Uncertain DTW
        DTS_F=normrnd(DTS_F,fit_S_int_Ampl/(2*1.95996)); %Uncertain DTS
        indx=find(DTS_F(:)<0);
        DTS_F(indx)=0;
        indx=find(DTW_F(:)<0);
        DTW_F(indx)=0;
        clear indx;
        Tw=normrnd(fit_W_phase,(fit_W_int_phase/(2*1.95996))); %Uncertain Tw
        Ts=normrnd(fit_S_phase,(fit_S_int_phase/(2*1.95996))); %Uncertain Ts
        LAGt_F=(Ts-Tw)*(15*60);%This correspond to Time Lag in seconds temporary
        indx=find(LAGt_F(:)<-1*minlag);
        [zr,zc]=find(LAGt_F<0);
        LAGt_F(indx)=86400+LAGt_F(indx);
        clear indx
        indx=find(LAGt_F(:)<minlag);
        LAGt_F(indx)=0;
        [zr,zc]=find(LAGt_F==0);
        zu=normrnd(z,z_uns/(2*1.95996)); %Uncertain z
        ku=normrnd(k,k_uns); %uncertain k
        a_F=(log10(DTS_F./DTW_F))/-zu;
        b_F=(2*pi*LAGt_F)/(tau*zu);
        v_F=ku*((b_F.^2)-(a_F.^2))./a_F;
        indx=find(DTS_F(:)<=minamp);
        v_F(indx)=-1.7E-3;
        q_F(:,:,it)=v_F*-thetha;
        [ri,ci,zi]=size(q_F);
        if it==iter;
            for f=1:ri;
                for ff=1:zi;
```

```
                q_Ft=q_F(f,:,ff);
                q_Ft=sort(q_Ft,2);
                q_Fnan=isnan(q_Ft);
                c_Fnan=sum(q_Fnan,2);
                if ff==1;
                   q=q_Ft(:,1:ci-c_Fnan);
                   qq.([char(81) int2str(f)])=q;
                else
                   q=[q q_Ft(:,1:ci-c_Fnan)];
                   q=sort(q);
                   qq.([char(81) int2str(f)])=q;
                   if ff==zi;
                      q_F_median(f,1)=median(q);
                      q_F_average(f,1)=mean(q);
                      q_F_var(f,1)=var(q);
                      q_F_n(f,1)=length(q);
                      q_F_std(f,1)=std(q);              %Standard Deviation
                      low(f,1)=ceil(0.025*(q_F_n(f,1)+1));   %low rank
                      hi(f,1)=floor(0.975*(q_F_n(f,1)+1));   %hi rank
                      zscore(f,1)=(q(hi(f,1))-q(low(f,1)))/2;%Distribution z score
                      SE(f,1)=q_F_std(f,1)/sqrt(q_F_std(f,1));%Standard Error
                      ConfInt(f,1)=zscore(f,1)*SE(f,1);
                   end;
                end;
             end;
          end;
          q40M=qq;
          R40M(:,12)=(sqrt(q_F_var)./sqrt(q_F_n-1)).*tinv(0.95,(q_F_n-
1));%95%Confidence Bounds T-dist
          R40M(:,11)=ConfInt;                          %95%Confidence Interval
unassumed dist
          R40M(:,9)=q_F_average;
          R40M(:,10)=q_F_median;
          R40M(:,13)=q_F_std;
          R40M(:,14)=q_F_n;
          clear DTW_F DTS_F Tw Ts LAGt_F a_F b_F v_F q_F_median q_F_average
...
             q_F_var q_F_n q_F q_F_std q_F low hi zscore SE ConfInt indx zr zcm zu ku
ri ci zi fit_S_int_Ampl...
             fit_W_int_Ampl fit_W_Ampl fit_S_Ampl fit_S_int_phase...
             fit_W_int_phase qq q
          disp('Done with scale:')
          disp(S)
          toc
```

```
            end;
        end
    end;
end;
```

APENDIX: MATLAB CODE TO APPLY BOOTSTRAP CONFIDENCE INTERVAL ANALYIS TO FLUX DISTRIBUTIONS

```
%% Boot MAR
clc
Ref=MAR10K;
for z=1:41
   if isfield(MAR10K_q, [char(81) int2str(z)])==0;
      break
   end;
   A1=MAR10K_q.([char(81) int2str(z)]);
   [r,c]=size(A1);
   CI_MAR10K(:,z)= bootci(10000,@median,A1);
end;
MAR10K(:,15:16)=CI_MAR10K';
MAR10K(:,17)=mean(MAR10K(:,15:16),2);
MAR10K(:,18)=MAR10K(:,15)-MAR10K(:,17);

%% Boot MAR
clc
Ref=MAR1K;
for z=1:41
   if isfield(MAR1K_q, [char(81) int2str(z)])==0;
      break
   end;
   A1=MAR1K_q.([char(81) int2str(z)]);
   [r,c]=size(A1);
   CI_MAR1K(:,z)= bootci(10000,@median,A1);
end;
MAR1K(:,15:16)=CI_MAR1K';
MAR1K(:,17)=mean(MAR1K(:,15:16),2);
MAR1K(:,18)=MAR1K(:,15)-MAR1K(:,17);

%% Boot MAR
clc
Ref=MAR100M;
for z=1:41
   if isfield(MAR100M_q, [char(81) int2str(z)])==0;
      break
   end;
   A1=MAR100M_q.([char(81) int2str(z)]);
   [r,c]=size(A1);
   CI_MAR100M(:,z)= bootci(10000,@median,A1);
end;
```

```
MAR100M(:,15:16)=CI_MAR100M';
MAR100M(:,17)=mean(MAR100M(:,15:16),2);
MAR100M(:,18)=MAR100M(:,15)-MAR100M(:,17);
%% Boot MAR
clc
Ref=MAR40M;
for z=1:41
   if isfield(MAR40M_q, [char(81) int2str(z)])==0;
      break
   end;
   A1=MAR40M_q.([char(81) int2str(z)]);
   [r,c]=size(A1);
   CI_MAR40M(:,z)= bootci(10000,@median,A1);
end;
MAR40M(:,15:16)=CI_MAR40M';
MAR40M(:,17)=mean(MAR40M(:,15:16),2);
MAR40M(:,18)=MAR40M(:,15)-MAR40M(:,17);

%%%%%%%%%%%%%%%%%%%%%%%%%%%%%%%%%%%%%%%%%%%%%%%%%%%%%%%%
%%%%%%%%%%%%%%%%%%%%%%%%%%%%%%%%%%%%%%%%%%
%% Boot MAY
clc
Ref=MAY10K;
for z=1:41
   if isfield(MAY10K_q, [char(81) int2str(z)])==0;
      break
   end;
   A1=MAY10K_q.([char(81) int2str(z)]);
   [r,c]=size(A1);
   CI_MAY10K(:,z)= bootci(10000,@median,A1);
end;
MAY10K(:,15:16)=CI_MAY10K';
MAY10K(:,17)=mean(MAY10K(:,15:16),2);
MAY10K(:,18)=MAY10K(:,15)-MAY10K(:,17);

%% Boot MAY
clc
Ref=MAY1K;
for z=1:41
   if isfield(MAY1K_q, [char(81) int2str(z)])==0;
      break
   end;
   A1=MAY1K_q.([char(81) int2str(z)]);
   [r,c]=size(A1);
```

```
    CI_MAY1K(:,z)= bootci(10000,@median,A1);
end;
MAY1K(:,15:16)=CI_MAY1K';
MAY1K(:,17)=mean(MAY1K(:,15:16),2);
MAY1K(:,18)=MAY1K(:,15)-MAY1K(:,17);

%% Boot MAY
clc
Ref=MAY100M;
for z=1:41
    if isfield(MAY100M_q, [char(81) int2str(z)])==0;
        break
    end;
    A1=MAY100M_q.([char(81) int2str(z)]);
    [r,c]=size(A1);
    CI_MAY100M(:,z)= bootci(10000,@median,A1);
end;
MAY100M(:,15:16)=CI_MAY100M';
MAY100M(:,17)=mean(MAY100M(:,15:16),2);
MAY100M(:,18)=MAY100M(:,15)-MAY100M(:,17);
%% Boot MAY
clc
Ref=MAY40M;
for z=1:41
    if isfield(MAY40M_q, [char(81) int2str(z)])==0;
        break
    end;
    A1=MAY40M_q.([char(81) int2str(z)]);
    [r,c]=size(A1);
    CI_MAY40M(:,z)= bootci(10000,@median,A1);
MAY40M(:,15:16)=CI_MAY40M';
MAY40M(:,17)=mean(MAY40M(:,15:16),2);
MAY40M(:,18)=MAY40M(:,15)-MAY40M(:,17);

%%%%%%%%%%%%%%%%%%%%%%%%%%%%%%%%%%%%%%%%%%%%%%%%%%%%%%%%%%%%%%%%%%%%%%%%
%%%%%%%%%%%%%%%%%%%%%%%%%%%%%%%%%%%%%%%%%%%%%%%%%%%%%%%%%%%%%%%%%%%%%%%%
%% Boot NOV
clc
Ref=NOV10K;
for z=1:41
    if isfield(NOV10K_q, [char(81) int2str(z)])==0;
        break
    end;
    A1=NOV10K_q.([char(81) int2str(z)]);
```

```
    [r,c]=size(A1);
    CI_NOV10K(:,z)= bootci(10000,@median,A1);
end;
NOV10K(:,15:16)=CI_NOV10K';
NOV10K(:,17)=mean(NOV10K(:,15:16),2);
NOV10K(:,18)=NOV10K(:,15)-NOV10K(:,17);

%% Boot NOV
clc
Ref=NOV1K;
for z=1:41
    if isfield(NOV1K_q, [char(81) int2str(z)])==0;
        break
    end;
    A1=NOV1K_q.([char(81) int2str(z)]);
    [r,c]=size(A1);
    CI_NOV1K(:,z)= bootci(10000,@median,A1);
end;
NOV1K(:,15:16)=CI_NOV1K';
NOV1K(:,17)=mean(NOV1K(:,15:16),2);
NOV1K(:,18)=NOV1K(:,15)-NOV1K(:,17);

%% Boot NOV
clc
Ref=NOV100M;
for z=1:41
    if isfield(NOV100M_q, [char(81) int2str(z)])==0;
        break
    end;
    A1=NOV100M_q.([char(81) int2str(z)]);
    [r,c]=size(A1);
    CI_NOV100M(:,z)= bootci(10000,@median,A1);
end;
NOV100M(:,15:16)=CI_NOV100M';
NOV100M(:,17)=mean(NOV100M(:,15:16),2);
NOV100M(:,18)=NOV100M(:,15)-NOV100M(:,17);
%% Boot NOV
clc
Ref=NOV40M;
for z=1:41
    if isfield(NOV40M_q, [char(81) int2str(z)])==0;
        break
    end;
    A1=NOV40M_q.([char(81) int2str(z)]);
```

```
    [r,c]=size(A1);
    CI_NOV40M(:,z)= bootci(10000,@median,A1);
end;
NOV40M(:,15:16)=CI_NOV40M';
NOV40M(:,17)=mean(NOV40M(:,15:16),2);
NOV40M(:,18)=NOV40M(:,15)-NOV40M(:,17);

%%%%%%%%%%%%%%%%%%%%%%%%%%%%%%%%%%%%%%%%%%%%%%%%%%%%%%%%%%%%%%%%%%%%%%%%%%%%%%%%%%%%%%%%%%%%%%%%%%%%%%%%%%%%%%%%%%%%%%%%%%%%
%% Boot APR
clc
Ref=APR10K;
for z=1:41
    if isfield(APR10K_q, [char(81) int2str(z)])==0;
        break
    end;
    A1=APR10K_q.([char(81) int2str(z)]);
    [r,c]=size(A1);
    CI_APR10K(:,z)= bootci(10000,@median,A1);
end;
APR10K(:,15:16)=CI_APR10K';
APR10K(:,17)=mean(APR10K(:,15:16),2);
APR10K(:,18)=APR10K(:,15)-APR10K(:,17);

%% Boot APR
clc
Ref=APR1K;
for z=1:41
    if isfield(APR1K_q, [char(81) int2str(z)])==0;
        break
    end;
    A1=APR1K_q.([char(81) int2str(z)]);
    [r,c]=size(A1);
    CI_APR1K(:,z)= bootci(10000,@median,A1);
end;
APR1K(:,15:16)=CI_APR1K';
APR1K(:,17)=mean(APR1K(:,15:16),2);
APR1K(:,18)=APR1K(:,15)-APR1K(:,17);

%% Boot APR
clc
Ref=APR100M;
for z=1:41
    if isfield(APR100M_q, [char(81) int2str(z)])==0;
```

```
        break
    end;
    A1=APR100M_q.([char(81) int2str(z)]);
    [r,c]=size(A1);
    CI_APR100M(:,z)= bootci(10000,@median,A1);
end;
APR100M(:,15:16)=CI_APR100M';
APR100M(:,17)=mean(APR100M(:,15:16),2);
APR100M(:,18)=APR100M(:,15)-APR100M(:,17);
%% Boot APR
clc
Ref=APR40M;
for z=1:41
    if isfield(APR40M_q, [char(81) int2str(z)])==0;
        break
    end;
    A1=APR40M_q.([char(81) int2str(z)]);
    [r,c]=size(A1);
    CI_APR40M(:,z)= bootci(10000,@median,A1);
end;
APR40M(:,15:16)=CI_APR40M';
APR40M(:,17)=mean(APR40M(:,15:16),2);
APR40M(:,18)=APR40M(:,15)-APR40M(:,17);
```

REFERENCES

Anderson, M. P. (2005), Ground Water; Heat as a ground water tracer.(Review Paper), *43*, 951(18).

Baillie, M. N., J. F. Hogan, B. Ekwurzel, A. K. Wahi, and C. J. Eastoe (2007), Quantifying water sources to a semiarid riparian ecosystem, San Pedro River, Arizona, *J. Geophys. Res. (G Biogeosci.), 112*.

Becker, M. W., T. Georgian, H. Ambrose, J. Siniscalchi, and K. Fredrick (2004), Estimating flow and flux of ground water discharge using water temperature and velocity, *J. Hydrol. (Amst.), 296*, 221-233.

Blasch, K. W., T. P. A. Ferre, and J. P. Hoffmann (2005), A statistical technique for interpreting streamflow timing using streambed sediment thermographs, *Vadose Zone Journal, 3*, 936-946.

Bonett, D. G. and R. M. Price (2002), Statistical inference for a linear function of medians: Confidence intervals, hypothesis testing, and sample size requirements, *Psychol. Methods, 7*, 370-383.

Brooks, P. D. and M. M. Lemon (2007), Spatial variability in dissolved organic matter and inorganic nitrogen concentrations in a semiarid stream, San Pedro River, Arizona, *Journal of Geophysical Research-Biogeosciences, 112*, G03S05.

Coes, A. L. and D. R. Pool (2005), Ephemeral-stream channel and basin-floor infiltration and recharge in the Sierra Vista subwatershed of the Upper San Pedro Basin, southeastern Arizona: U.S. Geological Survey Open-File Report, *2005-1023*(U.S. Geological Survey Open-File Report), 67 p.

Conant, B.,Jr (2004), Delineating and Quantifying Ground Water Discharge Zones Using Streambed Temperatures, *Ground Water, 42*, 243-257.

Constantz, J., A. E. Stewart, R. Niswonger, and L. Sarma (2002), Analysis of temperature profiles for investigating stream losses beneath ephemeral channels, *Water Resour. Res., 38*.

Dent, C. L. and N. B. Grimm (1999), Spatial heterogeneity of stream water nutrient concentrations over successional time, *Ecology, 80*, 2283-2298.

Dent, C. L., N. B. Grimm, and S. G. Fisher (2001), Multiscale effects of surface-subsurface exchange on stream water nutrient concentrations, *J. N. Am. Benthol. Soc., 20*, 162-181.

Efron, B. and R. Tibshirani (1986), Bootstrap Methods for Standard Errors, Confidence Intervals, and Other Measures of Statistical Accuracy*, Statistical Science, 1*, 54-75.

Fisher, S. G. and W. L. Minckley (1978), Chemical Characteristics of a Desert Stream in Flash Flood*, Journal of Arid Environments, 1*, 25-33.

Grimm, N. B., H. M. Valett, E. H. Stanley, and S. G. Fischer (1991), Contribution of the Hyporheic Zone to Stability of an Arid-Land Stream*, Internationale Vereinigung fuer Theoretische und Angewandte Limnologie.Verhandlungen IVTLAP, p 1595-1599*, 23 ref. NSF Grant Nos. BSR 84-06891 and BSR 88-18612.

Grimm, N. B. (1987), Nitrogen Dynamics During Succession in a Desert Stream*, Ecology, 68*, 1157-1170.

Harvey, J. W. and K. E. Bencala (1993), Effect of Streambed Topography on Surface-Subsurface Water Exchange in Mountain Catchments*, Water Resources Research WRERAQ, p 89-98*, 38 ref.

Hatch, C. E., A. T. Fisher, J. Constantz, C. R. Ruehl, M. Los Huertos, G. Stemler, A. Rich, and C. Shennan (2006)*, Streambed Seepage and Implications for Local Hydrology: Time Series Analysis of Streambed Thermal Records and Other Methods Applied to a Strongly-Losing Stream*, American Geophysical Union Fall Meeting, San Francisco (USA), 11-15 Dec 2006, American Geophysical Union, 2000 Florida Ave., N.W. Washington DC 20009 USA, [URL:http://www.agu.org].

Hereford, R. (1993), Entrenchment and widening of the upper San Pedro River, Arizona*, Geological Society of America Special Paper, 282*, 1-46.

Holmes, R. M., S. G. Fisher, and N. B. Grimm (1994), Parafluvial nitrogen dynamics in a desert stream ecosystem*, J. N. Am. Benthol. Soc., 13*, 468-478.

Johnson, A. N., B. R. Boer, W. W. Woessner, J. A. Stanford, G. C. Poole, S. A. Thomas, and S. J. O'Daniel (2005), Evaluation of an Inexpensive Small-Diameter Temperature Logger for Documenting Ground Water-River Interactions*, Ground Water Monit. Remediat., 25*, 68-74.

Jones, J. B.,Jr, S. G. Fisher, and N. B. Grimm (1995a), Nitrification in the hyporheic zone of a desert stream ecosystem*, J. N. Am. Benthol. Soc., 14*, 249-258.

Jones, J. B.,Jr, S. G. Fisher, and N. B. Grimm (1995b), Nitrification in the hyporheic zone of a desert stream ecosystem*, J. N. Am. Benthol. Soc., 14*, 249-258.

Jones, J. B.,Jr, S. G. Fisher, and N. B. Grimm (1995c), Vertical hydrologic exchange and ecosystem metabolism in a Sonoran Desert stream*, Ecology, 76*, 942-952.

Keery, J., A. Binley, N. Crook, and J. W. N. Smith (2007), Temporal and spatial variability of groundwater-surface water fluxes: Development and application of an analytical method using temperature time series*, J. Hydrol. (Amst.), 336*, 1-16.

Loheide, S. P.,II and S. M. Gorelick (2006), Quantifying Stream-Aquifer Interactions through the Analysis of Remotely Sensed Thermographic Profiles and In Situ Temperature Histories*, Environ. Sci. Technol., 40*, 3336-3341.

Plummer, L. N., L. M. Bexfield, S. K. Anderholm, W. E. Sanford, and E. Busenberg (2004), Hydrochemical tracers in the middle Rio Grande Basin, USA: 1. Conceptualization of groundwater flow*, Hydrogeol. J., 12*, 359-388.

Pool, D. R. and A. L. Coes (1999), Hydrogeologic investigations of the Sierra Vista subwatershed of the Upper San Pedro Basin, Cochise County, southeast Arizona: Water Resources Investigation Report*, 99-4197*, 41 p.

Rossi, R. E., D. J. Mulla, A. G. Journel, and E. H. Franz (1992), Geostatistical Tools for Modeling and Interpreting Ecological Spatial Dependence*, Ecol. Monogr., 62*, 277-314.

Selker, J. S., L. Thevenaz, H. Huwald, A. Mallet, W. Luxemburg, N. Van de Giesen, M. Stejskal, J. Zeman, M. Westhoff, and M. B. Parlange (2006), Distributed fiber-optic temperature sensing for hydrologic systems*, Water Resour. Res., 42*.

Silliman, S. E., J. Ramirez, and R. L. McCabe (1995), Quantifying downflow through creek sediments using temperature time series: One-dimensional solution incorporating measured surface temperature*, J. Hydrol. (Amst.), 167*, 99-119.

Silliman, S. E. and D. F. Booth (1993), Analysis of time-series measurements of sediment temperature for identification of gaining vs. losing portions of Juday Creek, Indiana*, Journal of Hydrology, 146*, 131-148.

Stallman, R. W. (1965), Steady 1-Dimensional Fluid Flow in a Semi-Infinite Porous Medium with Sinusoidal Surface Temperature*, Journal of Geophysical Research, 70*, 2821-2827.

Suzuki, S. (1960), Percolation Measurements Based on Heat Flow through Soil with Special Reference to Paddy Fields*, Journal of Geophysical Research, 65*, 2883-2885.

Valett, H. M., S. G. Fisher, and E. H. Stanley (1990), Physical and Chemical Characteristics of the Hyporheic Zone of a Sonoran Desert Stream*, Journal of the North American Benthological Society JNASEC, p 201-215*, 57 ref. NSF Grants BSR 84.

Valett, H. M., S. G. Fisher, N. B. Grimm, and P. Camill (1994), Vertical Hydrologic Exchange and Ecological Stability of a Desert Stream Ecosystem*, Ecology, 75*, 548-560.

Wahi, A. K., J. F. Hogan, B. Ekwurzel, M. N. Baillie, and C. J. Eastoe (2008), Geochemical Quantification of Semiarid Mountain Recharge*, Ground Water*, doi: 10.1111/j.1745-6584.2007.00413.x.